

BENCE BÉRI
THESIS WORK

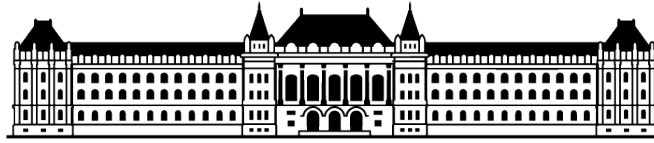
"All models are wrong, but some are useful."

George Box (1976)

BUDAPEST UNIVERSITY OF TECHNOLOGY AND ECONOMICS
FACULTY OF MECHANICAL ENGINEERING
DEPARTMENT OF APPLIED MECHANICS



THESIS WORK



BUDAPEST UNIVERSITY OF TECHNOLOGY AND ECONOMICS
FACULTY OF MECHANICAL ENGINEERING
DEPARTMENT OF APPLIED MECHANICS

BENCE BÉRI
THESIS

Bending vibrations of cantilever beams under
combined loads

Supervisor:

Prof. Gábor Stépán
Head of Department

Consultant:

Prof. John Hogan
Professor of Mathematics

BUDAPEST, 2017

NYILATKOZATOK

Elfogadási nyilatkozat

Ezen diplomaterv a Budapesti Műszaki és Gazdaságtudományi Egyetem Gépészmérnöki Kara által a Diplomatervezési feladatra előírt valamennyi tartalmi és formai követelményeknek, továbbá a feladatkiírásban előírtaknak maradéktalanul eleget tesz. E diplomatervet a nyilvános bírálatra és nyilvános előadásra alkalmasnak tartom.

Beadás időpontja: 2017. június 6.

Témavezető

Nyilatkozat az önálló munkáról

Alulírott *Béri Bence* (B6S8J0) a Budapesti Műszaki és Gazdaságtudományi Egyetem hallgatója, büntetőjogi és fegyelmi felelősségem tudatában kijelentem és sajátkezű aláírással igazolom, hogy a diplomatervet meg nem engedett segítség nélkül, saját magam készítettem, és dolgozatomban csak a megadott forrásokat használtam fel. Miden olyan részt, melyet szó szerint vagy azonos értelemben, de átfogalmazva más forrásból átvettem, egyértelműen, a hatályos előírásoknak megfelelően, a forrás megadásával megjelöltem.

Budapest, 2017. június 6.

Szigorló hallgató

Acknowledgement

I would first like to thank my thesis supervisor Prof. Gábor Stépán who had supported me professionally and he had provided help to work the topic out. I would also like to thank my thesis consultant Prof. John Hogan of the Department of Engineering Mathematics at University of Bristol for providing mathematical support in complicated mechanical problems.

Budapest, 2017. június 6.

Bence Béri

Contents

Introduction	3
1 Mechanical Modelling	7
1.1 Equations of the Global System	7
1.1.1 General Approaches	8
1.1.2 Application of torsion	9
1.2 Structural Stability of the System	14
1.2.1 Buckling by Compression	14
1.2.2 Buckling by Tension	17
1.2.3 Buckling by axial Torsion	18
1.2.4 Buckling by semi-tangential Torsion	21
1.2.5 Buckling by axial Torsion and Compression	22
1.2.6 Buckling by axial Torsion and Tension	24
1.2.7 Buckling by semi-tangential Torsion and Compression	24
1.2.8 Buckling by semi-tangential Torsion and Tension	26
1.3 Deformation functions	26
1.3.1 Compressed beam	26
1.3.2 Beam in Tension	28
1.3.3 Beam subjected to axial Torsion	29
1.3.4 Beam subjected to semi-tangential Torsion	32
1.3.5 Beam subjected to axial Torsion and Compression	34
1.3.6 Beam subjected to semi-tangential Torsion and Compression	35
1.3.7 Beam subjected to axial Torsion and Tension	36
1.3.8 Beam subjected to semi-tangential Torsion and Tension	37
1.4 Displacement Analysis by Energy Approach	37
2 Dynamical Behaviour	42
2.1 Approximating inertial effects	43
2.2 Natural frequencies of the cantilever beam	44
2.2.1 Vibration of unloaded beam	45
2.2.2 Beam in Compression	49

2.2.3	Beam in Tension	58
2.2.4	Twisted Beam	60
2.2.5	Twisted and Compressed Beam	63
2.2.6	Twisted and Tensed Beam	65
3	Investigation of a light rotating beam	67
3.1	Modelling	67
3.2	Stability	70
3.3	Results	71
4	Laboratory tests	74
4.1	Bifurcation diagram	75
4.2	Experimental results	80
	Summary	83
	Összefoglalás	85

List of Symbols

The notation of the given quantities - if it is possible - corresponds with the symbols of the national and international literatures. The rarely applied explanation of notations can be found at their first attendance.

Latin letters

Notation	Designation	Unit
a	Thickness of the cross section	m
A	Area of the cross section	m ²
b	Width of cross section	m
\mathbf{C}	Compliance matrix	SI
d	Complex function	SI
E	Young's modulus	GPa
f_i	Natural frequency	Hz
g	Gravitational acceleration (9.81)	m/s ²
I	Second moment	m ⁴
L	Length of the beam	m
m	Mass	kg
M	Bending moment function	Nm
M_t	Torsional moment	Nm/rad
\mathbf{M}	Mass matrix	SI
\mathbf{M}_t	Torsional moment vector	Nm/rad
P	Compressive force	N
\mathbf{q}	Vector of generalized coordinates	SI
\mathbf{Q}	Lateral force	N
r	Radius of the cross section	m
s	Spring stiffness	N/m
\mathbf{S}	Spring stiffness matrix	SI
t	Time	s
T	Kinetic energy	J
u	Displacement function in the direction x	m
U	Potential, strain energy	J
v	Displacement function in the direction y	m
\mathbf{v}	Velocity vector	m/s
w	Displacement function in the direction z	m
W_{ij}	Work of external forces	J

Greek letters

Notation	Designation	Unit
α	Torsional constant	SI
γ	Compression constant	SI
δ_v	End-displacement in the direction y (3D)	m
δ_w	End-displacement in the direction z (3D)	m
θ_C	Mass moment of inertia	kgm ²
ρ	Density of rod	kg/m ³
ω_n	Natural angular frequency	rad/s
Ω	Angular velocity	rad/s

Introduction

Manufacturing is called a process that transforms mouldings or raw materials to final products through different kinds of steps. The manufacturing process begins with the preparation of the materials whereby the designed component will be made. These materials are then modified through manufacturing processes to become the required part [24]. Machining is the most important type of forming where the typical cutting processes are defined as turning, milling and drilling. However, this method of production has significantly changed over the recent decades due to the increased requirements.

During manufacturing processes, unexpected vibrations called chatter might occur that generally result in noise or tool break and affect the shaped surfaces. Vibrations correspond to the relative displacement between the cutting tool and the workpiece and might be separated to two types of sources: forced and self-excited vibrations [31]. The forced vibrations are mainly caused by interrupted cutting, runout or external excitations. The self-excited vibrations are mostly related to the actual cutting depth and the relative position between the tool and the workpiece during the previous passage. These kinds of vibrations either disappear by itself or increase up to levels which seriously degrade the surface quality. Although there exist some mathematical models that make it possible to simulate the vibrations during machining but in practice is always more difficult to avoid vibrations [24].

Our investigation examines long boring tools and milling cutters that are subjected to compression/tension, twist and lateral forces originated in the process. The purpose is to predict how the each and combined loads affect the natural frequencies of the system, which could be useful in practice. As an industrial example, consider the moulding of a cylinder head where one of the manufacturing steps is the drilling of the bearing support of the camshaft called bearing street. It consists of more sliding bearings which are processed by a one piece drilling tool because concentricity is needed. The first bearing bore hole means the critical case due to the sensitivity to accidental buckling of the tool, since there is no support along the tool till its clamped end.

The objective of this work is to deal with one of the classical problems of mechanics that involves questions related to the theory of vibrations and strength of materials. The tool is modelled by a cantilever beam where the beam is considered to be prismatic, homogeneous, linearly elastic and inextensible. Apparently different mathematical correspondences can be determined between the general load cases and either the typical displacements or angular rotations of the beam section that describe the deflection of the beam. If we apply loading forces and torques at the same time then we can use the principle of superposition. The total strain can be calculated in turn by the summation of the caused strains of each load. In principle, these deformation expressions are called as beam design formulas [21].

Let us investigate a cantilever beam that is loaded by a simple lateral force at its free end. The linear theory of strength of materials only takes into account the displacement in the applied force direction, which does not correspond to the reality. As an example (see Fig. 1), consider an apple attached to the branch by means of the stem [9]. The mass of the stem is negligible compared to that of the apple. The stem is elastic and the natural frequency of the apple depends on the lateral deformation of the stem, which is affected by the tension caused by the weight of the fruit. During the linear vibration of the apple, the change of the potential energy related to the vertical position of its centre of gravity should be taken into account due to the deformation of the stem: the vertical displacement is a second degree function of the lateral displacement, similarly to the planar pendulum.

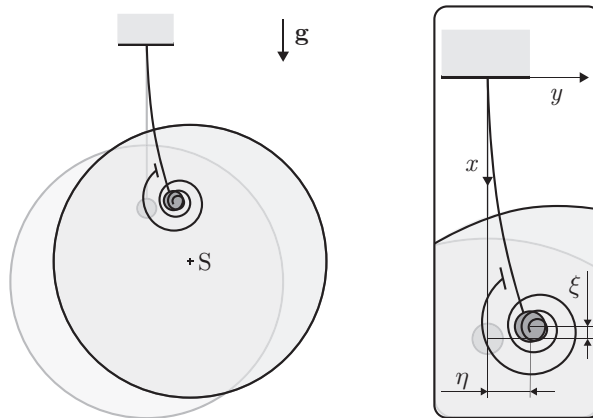


Figure 1: The mechanical model of the apple.

According to the theory applied for the stem, one can state the stiffness of a rod can be defined by an equivalent lateral spring stiffness. The stiffness is determined by means of a cantilever beam loaded by a lateral force at

its free end. The ratio of the force and the end displacement in the force direction caused by the force itself provides a stiffness formula. So there is another phenomenon that might be taken into account in natural frequency calculations, namely that the tensile force caused by the weight of the apple at the end of the stem results in the variation of the lateral spring stiffness of the stem. Further clarification is needed to discuss the two kinds of potential energy variations and their effects on the natural frequency.

To support the calculation of the potential energy, we are going to provide a simple analytic formula that describes the connection of the lateral and horizontal displacements of an elastic beam. There have been many related results in the literature: Borboni, De Santis [8] and Lee [18] have investigated a cantilever beam under combined loads with Ludwick type material and provided a numerical algorithm to solve the problem. González and Llorca [12] examined a same problem in the case of linearly elastic curved beams and derived an implicit analytical expression that still requires the application of some numerical methods. Solano-Carrillo [25] has found relationship between the geometrical and material nonlinearities concerning a beam under combined loading and suggested a semi-exact solution.

The model used by Beléndez *et al.* [5] is exactly the one we described above. The mathematical model is obtained from the Euler-Bernoulli curvature and bending moment connection and considered large and small deflections. They investigated only the longitudinal displacement of the beam and do not take into account its connection with the lateral displacement. Their results were achieved by incorporating some numerical methods and these were also compared with experimental ones.

Since our aim is to create a mathematical model related to boring tools, we need to take into account the effect of the twisting torque, too. Buckling is not caused only by compression hence why a beam may also become unstable under the action of a torsional moment. This problem cannot be treated in two-dimension any more because if we are dealing only with the bending vibrations then it is necessary to find how the twisting moment influences the bending function, which actually results in a three-dimensional problem [3]. There have been some previous results associated with the stability of these structures that mainly explain only the problem of the basic pinned-pinned constrained beam. Greenhill was the first who had attempted to find a solution for the case of cantilever shafts [14] because it is important for the design of turbines, generators and other rotating machinery. These results were improved by Ziegler [30] and Beck [4] later.

We are going to investigate distinct loading types including torsion and compression/tension: how they affect the stability of the rod, how the deformation will look like. Based on the deformation functions, the natural

frequencies of the given systems can be calculated through the variation of the potential energy. Eventually, we can compare how each load influences the stiffness of the system and how these forces cause the modification of the natural frequencies.

Since the boring and milling tools are rotating during the manufacturing process, we need to consider a rotating, compressed and twisted beam and determine the stability boundaries of the system. According to a related result by Wang [29], a light rotating column with a concentrated mass attached to its end that is able to model compression, might be treated by arc-length parameterization and varying boundary conditions. We are going to generalise the result when twist also appears.

Chapter 1

Mechanical Modelling

The hierarchy of the present mechanical modelling is manifested by different load types of a cantilever beam. The investigation of the models consists of two well separated phases in the sense of the theory of Strength of Materials. The first part is about the structural stability of the beam considered by equilibrium (and kinetic) approach(es) [30]. We elaborate on three cases including compressed/tensed, twisted and mixed load type beams. At the first two cases, we will provide two methods with different numbers of boundary conditions depending on whether real or complex valued differential equations are used. In the mixed type cases only the complex approach is used because of its compact mathematical presentation. The second part is about the general solutions of the three cases, but in this section we apply an additional lateral force at the free end of the beam in order to be able to examine the lateral stiffness of the system. Eventually, we give an analytical formula for the problem of compressed/tensed beam that is able to describe the connection between the lateral and horizontal displacements of the end point of the beam.

1.1 Equations of the Global System

The well-known mathematical model that describes beam deflections under bending had been given by the Euler-Bernoulli theory [3]. The governing equation of an elastic beam assumes the form

$$\frac{1}{\rho} = -\frac{M}{IE}, \quad (1.1)$$

where the radius of beam curvature at a certain cross section is denoted by ρ , IE is the bending stiffness, and the bending moment M is considered to

be positive if the upper fibre of the beam is in tension. The curvature can be expressed as

$$\frac{1}{\rho} = \frac{y''(x)}{(1 + (y'(x))^2)^{\frac{3}{2}}} = y''(x) \left(1 - \frac{3}{2} (y'(x))^2 \pm \dots \right) \quad (1.2)$$

where the primes mean the first and the second derivatives of the displacement function $y(x)$ with respect to the longitudinal coordinate x . If we assume small deflections of the beam, we may use the linear approximation

$$\frac{1}{\rho} \cong y''(x) \quad (1.3)$$

that yields the linearised form of Eq. (1.1):

$$\frac{\partial^2 y(x)}{\partial x^2} = -\frac{M(x)}{IE}, \quad (1.4)$$

where $M(x)$ describes the bending moment function, while IE is constant for the prismatic beam [21].

1.1.1 General Approaches

There exist many distinct approaches to investigate stability problems. We will consider only two of these that are going to be mentioned in buckling problems.

Equilibrium Approach:

The stability problem might be approached in different ways. One of them is called equilibrium approach [30]. Let us consider Fig. 1.1 which depicts a point mass that is able to move on the surface of a parabola without friction. If we assume that the motion occurs only in the $x - z$ plane then its equation is $z = \frac{1}{2}nx^2$. Apparently, the only equilibrium position ($x = 0$) is stable for $n > 0$, becomes neutral for $n = 0$ and unstable for $n < 0$.

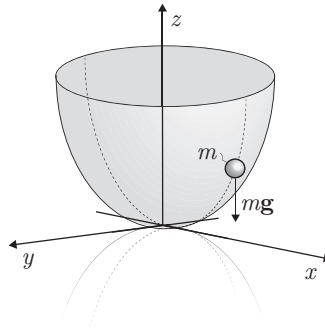


Figure 1.1: Motion of a point mass on a parabola.

When $n = 0$, the shape of the parabola coincides with the x axis and any point $x \neq 0$ on it represents non-isolated equilibrium positions. So the loss of the stability of the trivial equilibrium position is implied by the appearance of the non-isolated equilibrium positions in its neighbourhood.

So this approach is based on the observation that the transition from stability to instability of an equilibrium configuration may be marked by the appearance of additional nontrivial equilibrium configurations in the vicinity of the trivial one [3].

Kinetic Approach:

While the equilibrium approach has a simply static character, the present investigation is kinetic. The purpose of the kinetic approach is to figure out whether the small perturbations of the equilibrium result in increasing motions or not, which is an idea that leads to the definition of stability.

As an example, let us consider Fig. 1.1 again. The linearised differential equation of motion of the particle is described by

$$\ddot{x} + ngx = 0.$$

Since we know that $x = 0$ is the equilibrium position of the system, which can also be obtained from the differential equation of the motion of the particle, it is stable when $n > 0$. Hence we once more obtained the stability condition [30].

1.1.2 Application of torsion

Axial torsion:

In view of Eq. (1.4) we are already able to describe the system shown in Fig. 1.2, which is subjected to the twisting torque \mathbf{M}_t , compression \mathbf{P} , lateral force \mathbf{Q} with its two components Q_y , Q_z and bending moment \mathbf{M} with the components M_y , M_z . The cantilever prismatic beam has length L , it is inextensible and its bending stiffness is IE that is considered to be the same in both directions (y , z) when a twisting moment is applied. In case of compression only ($\mathbf{M}_t = 0$), the bending stiffness is not necessarily symmetric cylindrically since the problem becomes decoupled in the planes $(x - y)$ and $(x - z)$.

Let us consider that $v(x)$ is the displacement function in the direction y and $w(x)$ in the direction z . The deformation must be expected as a spatial curve characterized by the the functions of v and w . Considering the cross section A in Fig. 1.2 b) after buckling, the principal axes are represented by $\zeta_{1,2,3}$. Accordingly, ζ_1 defines the tangent of the deflected beam, and due to

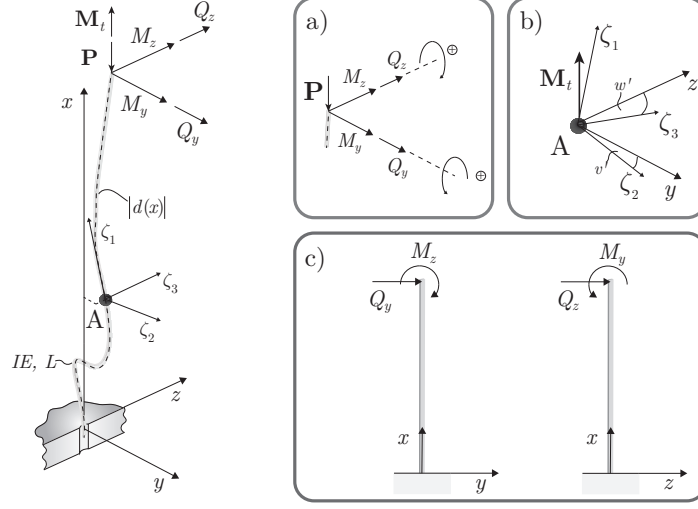


Figure 1.2: The mechanical model of a cantilever beam under combined loads.

the cylindrical symmetry of the cross section, ζ_2 can be considered to be parallel to the $(x - y)$ plane and ζ_3 to be parallel to the $(x - z)$ plane. Hence by resolving the torsional moment \mathbf{M}_t with respect to the principal system, we obtain two bending components with magnitude $-M_t \partial w(x) / \partial x$ in the direction y and $-M_t \partial v(x) / \partial x$ in the direction z [27]. The variation of the twisting moment (the projection of \mathbf{M}_t to ζ_1) is of second order, the torsional stiffness of the beam is irrelevant from the viewpoint of buckling [3]. Therefore the bending moment functions of the beam can be expressed as

$$\begin{aligned} M^{(z)}(x) &= M_t \frac{\partial w(x)}{\partial x} - M_z + Q_y(x - L) + Pv(x) - P\delta_v, \\ M^{(y)}(x) &= -M_t \frac{\partial v(x)}{\partial x} + M_y + Q_z(x - L) + Pw(x) - P\delta_w, \end{aligned} \quad (1.5)$$

and the governing equations assume the form

$$IE \frac{\partial^2 v(x)}{\partial x^2} + M_t \frac{\partial w(x)}{\partial x} + Pv(x) = M_z + Q_y(L - x) + P\delta_v, \quad (1.6)$$

$$IE \frac{\partial^2 w(x)}{\partial x^2} - M_t \frac{\partial v(x)}{\partial x} + Pw(x) = -M_y + Q_z(L - x) + P\delta_w, \quad (1.7)$$

where $\delta_v = v(L)$ and $\delta_w = w(L)$ denote the displacements at the end point of the rod. Henceforward, we deal with these second order coupled, non-homogeneous differential equations.

(Note that \mathbf{M}_t is a circulatory load, that is, its work does not equal to its potential. In a rotation through π about axis x , the work of \mathbf{M}_t is

positive. In two performed rotations through π about axes y and z , the same final position is reached, but now the work of \mathbf{M}_t is zero. Hence the literature [3][30] considers the axial torsion as a non-conservative load in the arrangement of the cantilever beam.)

Semi-tangential torsion:

It is necessary to investigate the way in which the torsional torque is transmitted to the beam. The reason why we are doing this will be explained in Subsec. 1.2.3. For example, twisting moment appears during the operation of a boring tool or a milling tool, but it is not obvious whether this moment is constant in the axial direction. There may be forces that make up couples that give rise to torsional moment vector with constant direction [30], but there may be others that will change direction together with the lateral deflection of the beam.

Let us consider a cantilever beam with cylindrically symmetric cross section depicted in Fig. 1.3 a). A tool-shaped disk (its height and mass are irrelevant here) is attached to the free end at point A. To describe the behaviour of the system, we have to take into account the strings of length a that are actually the levers of forces F . First, let us consider the two strings that are acted upon by the two forces F parallel to the axis z only. Generally, the unit vector \mathbf{n} denotes the one that is tangential to the deflected beam at A and also normal to the cross section. In the special case of the two forces parallel to z , this is denoted by the unit vector \mathbf{n}' that is also normal to the plane containing the two strings a , but it remains in the plane $x - y$.

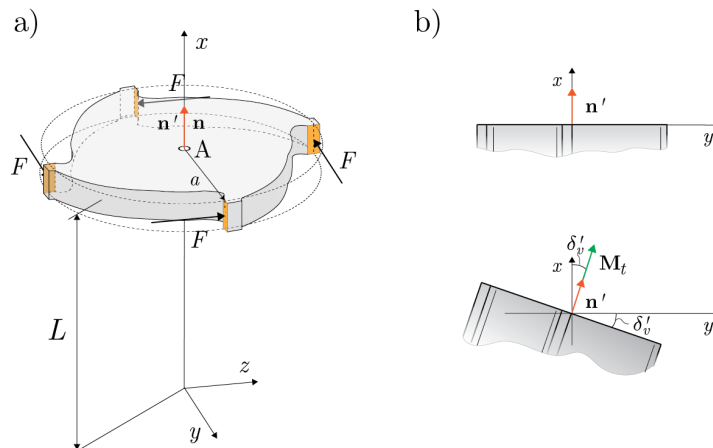


Figure 1.3: a) The arrangement of semi-tangential torque using a cylindrically symmetric cross section. b) The description of the quasi-tangential torque $\mathbf{M}_t = M_t \mathbf{n}'$ in case of two forces F only parallel to axis z where $\delta'_v = \partial v(x)/\partial x|_{x=L}$.

The difference between \mathbf{n} and \mathbf{n}' comes from the assumption that considers the forces F and thus the strings retain their directions during buckling. Before buckling, \mathbf{n} corresponds to $\mathbf{n}'^\top = (1 \ 0 \ 0)$; during buckling, it is not the case because \mathbf{n} is calculated by means of two rotations about the axes z and y . Therefore, we obtain

$$\mathbf{n} = \left(\begin{array}{c} \cos\left(\frac{\partial v(x)}{\partial x}\right) \cos\left(\frac{\partial w(x)}{\partial x}\right) \\ \sin\left(\frac{\partial v(x)}{\partial x}\right) \\ \cos\left(\frac{\partial v(x)}{\partial x}\right) \sin\left(\frac{\partial w(x)}{\partial x}\right) \end{array} \right) \Bigg|_{x=L} \cong \left(\begin{array}{c} 1 \\ \frac{\partial v(x)}{\partial x} \\ \frac{\partial w(x)}{\partial x} \end{array} \right) \Bigg|_{x=L}.$$

On contrary, in case of two forces F only parallel to axis z , the strings retain their direction during buckling, and the only motion that might occur is the rotation about axis z (see Fig. 1.3 b)), that is

$$\mathbf{n}' = \left(\begin{array}{c} \cos\left(\frac{\partial v(x)}{\partial x}\right) \\ \sin\left(\frac{\partial v(x)}{\partial x}\right) \\ 0 \end{array} \right) \Bigg|_{x=L} \cong \left(\begin{array}{c} 1 \\ \frac{\partial v(x)}{\partial x} \\ 0 \end{array} \right) \Bigg|_{x=L}.$$

Now, the moment vector is created by the two forces F , that is, $\mathbf{M}_t = M_t \mathbf{n}'$ where $M_t = 2Fa$ (see lower panel of Fig. 1.3 b)).

The case of all the four forces F is referred to as semi-tangential case (see Fig. 1.3 a)). Accordingly, $M_t = 4Fa$, which is the superposition of two couples $M_t/2$. Combining the previous case of two forces F parallel to z and two forces F parallel to y , the normal vector \mathbf{n} can be simply calculated. We have two moment vectors ($\mathbf{M}_t^{(1)}$, $\mathbf{M}_t^{(2)}$) that give

$$\begin{aligned} \mathbf{M}_t &= \mathbf{M}_t^{(1)} + \mathbf{M}_t^{(2)} \\ &= \frac{M_t}{2} \left(\begin{array}{c} 1 \\ \frac{\partial v(x)}{\partial x} \\ 0 \end{array} \right) \Bigg|_{x=L} + \frac{M_t}{2} \left(\begin{array}{c} 1 \\ 0 \\ \frac{\partial w(x)}{\partial x} \end{array} \right) \Bigg|_{x=L} = \frac{M_t}{2} \left(\begin{array}{c} 2 \\ \frac{\partial v(x)}{\partial x} \\ \frac{\partial w(x)}{\partial x} \end{array} \right) \Bigg|_{x=L}. \end{aligned} \quad (1.8)$$

It can be proven that the semi-tangential moment can be obtained in the same form when the number of the forces is $n > 2$ and they are uniformly

distributed around the cross section [30, 4]. Eq. (1.8) results two additional terms into Eq. (1.5), that are

$$\begin{aligned}M^{(z)}(x) &= \dots - \frac{1}{2}M_t\delta'_w, \\M^{(y)}(x) &= \dots + \frac{1}{2}M_t\delta'_v,\end{aligned}\tag{1.9}$$

where $\partial v(x)/\partial x$ and $\partial w(x)/\partial x$ at the end of the beam are denoted by δ'_v and δ'_w , respectively (compare these to the beam deflections δ_v and δ_w in Eq. (1.5)).

(Note that Beck [4] had investigated this and other torques and claims that buckling by this type of torque is a conservative problem.)

1.2 Structural Stability of the System

This section examines how the stability of the structures is affected by the different load types based on the above defined equilibrium approach. The main issue is whether the system becomes unstable after a certain load or not. There are obviously more complicated cases where combined loads appear. Here, it is not enough to provide a critical value for each load because of their interplay.

1.2.1 Buckling by Compression

If a straight beam is long compared to the sizes of its cross section and it is loaded in its axis of the centre of gravity at the free end by an increasingly growing compressive force, then at a certain critical load, it will lose the stability of its straight equilibrium shape. Obviously, three modes can be defined. As long as the compression is smaller than its critical value, the beam will shorten but retain its straight shape. This is called stable configuration that might be checked by means of a small lateral force perturbation acting on the rod. It would cause deflection but when it stops acting, the rod gets back to its initial equilibrium configuration. If we apply the exact critical value of compression by using also the lateral force, then the rod retains its deflected shape. It is called neutrally stable position in linear approximation, but it can be weakly stable or unstable due to the nonlinearities. Eventually, the unstable mode might be achieved by a compression value larger than the critical one. Accordingly, the stability of the rod depends on the magnitude of compression that can be analysed by mathematical manners.

Let us consider two different mathematical approaches that consider modifications in the number of the boundary conditions and in the method of the solution. Based on Eq. (1.5), we obtain a simple two-dimensional problem considering $M_t = 0$, $M_{y,z} = 0$ and $Q_{y,z} = 0$:

$$\frac{\partial^2 v(x)}{\partial x^2} + \gamma v(x) = \gamma \delta_v, \quad \gamma = \frac{P}{IE}. \quad (1.10)$$

Case 1: Eq. (1.10) has a peculiar mathematical form since the end displacement of the beam $\delta_v = v(L)$ appears in the differential equation itself. Our aim is to eliminate this ill-defined form by using a fourth order governing equation, which seems to be obtainable from Eq. (1.10) by differentiating it twice with respect to x . The rigorous derivation of the fourth order form is based on the fact that while the bending moment is proportional to the second derivative in the curvature, the lateral distributed forces acting on the beam are the second derivatives of the bending moment itself. Consequently,

the connection between the lateral deformations and the lateral forces must be 4th order derivative:

$$\frac{\partial^4 v(x)}{\partial x^4} + \gamma \frac{\partial^2 v(x)}{\partial x^2} = 0, \quad (1.11)$$

with four boundary conditions

$$\begin{aligned} v(0) = \frac{\partial v(x)}{\partial x} \Big|_{x=0} = \frac{\partial^2 v(x)}{\partial x^2} \Big|_{x=L} = 0, \\ \frac{\partial^3 v(x)}{\partial x^3} \Big|_{x=L} = -\gamma \frac{\partial v(x)}{\partial x} \Big|_{x=L}. \end{aligned} \quad (1.12)$$

Eq. (1.11) can be transformed to a four dimensional first order system described by

$$\frac{\partial \mathbf{z}(x)}{\partial x} = \underbrace{\begin{pmatrix} 0 & 1 & 0 & 0 \\ 0 & 0 & 1 & 0 \\ 0 & 0 & 0 & 1 \\ 0 & 0 & -\gamma & 0 \end{pmatrix}}_{\mathbf{A}} \mathbf{z}(x), \quad (1.13)$$

where the new vector variable is

$$\mathbf{z}^\top(x) = \left(v(x) \quad \frac{\partial v(x)}{\partial x} \quad \frac{\partial^2 v(x)}{\partial x^2} \quad \frac{\partial^3 v(x)}{\partial x^3} \right).$$

To determine the general solution of the system, we need to calculate the eigenvalues and eigenvectors of matrix \mathbf{A} . It yields

$$\lambda_{1,2} = 0, \quad \lambda_{3,4} = \pm \sqrt{\gamma}i, \quad \mathbf{u}_1 = \begin{pmatrix} 1 \\ 0 \\ 0 \\ 0 \end{pmatrix}, \quad \mathbf{u}_3 = \bar{\mathbf{u}}_4 = \begin{pmatrix} 1 \\ \sqrt{\gamma}i \\ -\gamma \\ -\gamma\sqrt{\gamma}i \end{pmatrix}. \quad (1.14)$$

In case of $\lambda_{1,2}$, the geometrical multiplicity of the system is 1 and the algebraic is 2. Since algebraic multiplicity (k) of λ is greater than its geometrical multiplicity (l), thus besides the already given linearly independent eigenvectors, it is necessary to have even $(k - l) = 1$ linearly independent solutions. These might be found in the form

$$\boldsymbol{\eta}(x) = x e^{\lambda x} \boldsymbol{\xi} + e^{\lambda x} \boldsymbol{\zeta}.$$

If it is substituted into $\partial \boldsymbol{\eta}(x) / \partial x = \mathbf{A} \boldsymbol{\eta}(x)$, we obtain

$$e^{\lambda x} \boldsymbol{\xi} + x \lambda e^{\lambda x} \boldsymbol{\xi} + \lambda e^{\lambda x} \boldsymbol{\zeta} = \mathbf{A} e^{\lambda x} \boldsymbol{\xi} x + \mathbf{A} e^{\lambda x} \boldsymbol{\zeta}$$

that can be separated to

$$(\mathbf{A} - \lambda\mathbf{I})\boldsymbol{\xi} = 0, \quad (\mathbf{A} - \lambda\mathbf{I})\boldsymbol{\zeta} = \boldsymbol{\xi}$$

where $\boldsymbol{\xi}$ is an eigenvector and $\boldsymbol{\zeta}$ is a generalized eigenvector belonging to λ . Note, that $\boldsymbol{\zeta}$ does not belong to the characteristic subspace of λ because if it belonged to, the equation would present it. Thus the general solution is

$$v(x) = A + Bx + C \cos(\sqrt{\gamma}x) + D \sin(\sqrt{\gamma}x). \quad (1.15)$$

Considering the boundary conditions Eq. (1.12), the system of equations with respect to the unknown coefficients A, B, C, D can be expressed as

$$\begin{pmatrix} 1 & 0 & 1 & 0 \\ 0 & 1 & 0 & \sqrt{\gamma} \\ 0 & 0 & -\cos(\sqrt{\gamma}L) & -\sin(\sqrt{\gamma}L) \\ 0 & 1 & 0 & 0 \end{pmatrix} \begin{pmatrix} A \\ B \\ C \\ D \end{pmatrix} = \begin{pmatrix} 0 \\ 0 \\ 0 \\ 0 \end{pmatrix}. \quad (1.16)$$

The non-trivial solution leads to the determinant of the system matrix being equal to zero, which provides

$$\cos(\sqrt{\gamma}L)\sqrt{\gamma} = 0. \quad (1.17)$$

With integer n , this means

$$\sqrt{\gamma}L = (2n + 1)\frac{\pi}{2}. \quad (1.18)$$

When $n = 0$, we obtain the first critical value of compression

$$P_{\text{cr}} = \left(\frac{\pi}{2L}\right)^2 IE \quad (1.19)$$

that is called as Euler's critical load.

Case 2: This solution holds the constant term $\gamma\delta_v$ of Eq. (1.10) where $\delta_v = v(L)$, and it needs only two boundary conditions for the fixed end point of the beam:

$$v(0) = 0, \quad \left. \frac{\partial v(x)}{\partial x} \right|_{x=0} = 0. \quad (1.20)$$

By using the non-homogeneous term, the differential equation satisfies the boundary conditions that refer to the free end of the beam (see Eq. (1.12)). Due to the linear non-homogeneous nature of the differential equation, the solution consists of a homogeneous part and a particular one:

$$v(x) = v_{\text{H}}(x) + v_{\text{P}}(x).$$

The homogeneous part can be investigated by substituting the test function $v(x) = Ke^{\lambda x}$ into Eq. (1.10):

$$\underbrace{Ke^{\lambda x}}_{\neq 0}(\lambda^2 + \gamma) = 0 \quad \Rightarrow \quad \lambda_{1,2} = \pm\sqrt{\gamma}i, \quad (1.21)$$

that implies

$$v_H(x) = c_1e^{\lambda_1 x} + c_2e^{\lambda_2 x}.$$

Because the non-homogeneity is only a constant number, the general solution assumes the form

$$v(x) = A \cos(\sqrt{\gamma}x) + B \sin(\sqrt{\gamma}x) + \delta_v. \quad (1.22)$$

The unknown coefficients A, B have to be $A = -\delta_v$ and $B = 0$ in order to satisfy the boundary conditions (see Eq. (1.20)). Therefore, $v(x) = \delta_v(1 - \cos(\sqrt{\gamma}L))$, that is, if $v(L) = \delta_v$, then $\delta_v \cos(\sqrt{\gamma}L)$ must be zero. It implies the same solutions as above (see Eq. (1.18)).

If we consider δ_v as an unknown displacement of the end point of the beam in Eq. (1.22), then by using Eq. (1.20), the system of equations is

$$\begin{pmatrix} 1 & 0 & 1 \\ 0 & \sqrt{\gamma} & 0 \\ \cos(\sqrt{\gamma}L) & \sin(\sqrt{\gamma}L) & 0 \end{pmatrix} \begin{pmatrix} A \\ B \\ \delta_v \end{pmatrix} = \begin{pmatrix} 0 \\ 0 \\ 0 \end{pmatrix}. \quad (1.23)$$

The non-trivial solution of Eq. (1.23) also leads us to the same critical compressive loads as above (see Eq. (1.18)).

Note that in this case the equilibrium and kinetic approaches discussed in Subsec. 1.1.1 provide the same result. The solution of the kinetic approach can be found in [30] and it leads to the critical compressive load.

1.2.2 Buckling by Tension

Tension might be treated as a negative compression, however, the solution of the basic differential equation modifies. Based on Eq. (1.10), it is necessary to change the sign of P , which yields

$$\frac{\partial^2 v(x)}{\partial x^2} - \gamma v(x) = -\gamma \delta_v, \quad \gamma > 0.$$

The boundary conditions correspond to Eq. (1.20). Now, the homogeneous part of the solution is different. After the application of the test function, we obtain

$$\underbrace{Ke^{\lambda x}}_{\neq 0}(\lambda^2 - \gamma) = 0 \quad \Rightarrow \quad \lambda_{1,2} = \pm\sqrt{\gamma}.$$

So the general solution for tension is given by

$$v(x) = A \cosh(\sqrt{\gamma}x) + B \sinh(\sqrt{\gamma}x) + \delta_v,$$

that modifies the system of equations

$$\begin{pmatrix} 1 & 0 & 1 \\ 0 & \sqrt{\gamma} & 0 \\ \cosh(\sqrt{\gamma}L) & \sinh(\sqrt{\gamma}L) & 0 \end{pmatrix} \begin{pmatrix} A \\ B \\ \delta_v \end{pmatrix} = \begin{pmatrix} 0 \\ 0 \\ 0 \end{pmatrix}.$$

The non-trivial solution does not provide critical value for tension because the determinant $\sqrt{\gamma} \cosh(\sqrt{\gamma}L)$ of the system matrix cannot be zero.

Note that the kinetic approach would provide the same result similarly to the case of compression.

1.2.3 Buckling by axial Torsion

Buckling might take place not only by compression. The modelled cantilever beam is also able to buckle and become unstable by torsion. Let us investigate the problem similarly to Subsec. 1.2.1. Based on the equilibrium approach and Eqs. (1.6), (1.7), we obtain a second order differential equation system considering $P = 0$, $M_{y,z} = 0$ and $Q_{y,z} = 0$:

$$\left. \begin{aligned} \frac{\partial^2 v(x)}{\partial x^2} + \alpha \frac{\partial w(x)}{\partial x} &= 0 \\ \frac{\partial^2 w(x)}{\partial x^2} - \alpha \frac{\partial v(x)}{\partial x} &= 0 \end{aligned} \right\}, \quad \alpha = \frac{M_t}{IE}. \quad (1.24)$$

Case 1: Based on the statement that claims the second derivative of the bending moment function is proportional to the lateral distributed forces acting on the beam, we will have a fourth order differential equation system by differentiating Eq. (1.24) twice. Thus the boundary conditions are

$$\begin{aligned} v(0) = \frac{\partial v(x)}{\partial x} \Big|_{x=0} &= \frac{\partial^2 v(x)}{\partial x^2} \Big|_{x=L} = \frac{\partial^3 v(x)}{\partial x^3} \Big|_{x=L} = 0, \\ w(0) = \frac{\partial w(x)}{\partial x} \Big|_{x=0} &= \frac{\partial^2 w(x)}{\partial x^2} \Big|_{x=L} = \frac{\partial^3 w(x)}{\partial x^3} \Big|_{x=L} = 0. \end{aligned} \quad (1.25)$$

Eq. (1.24) can be converted to a first order system

$$\frac{\partial \mathbf{z}(x)}{\partial x} = \underbrace{\begin{pmatrix} 0 & 1 & 0 & 0 & 0 & 0 & 0 & 0 \\ 0 & 0 & 1 & 0 & 0 & 0 & 0 & 0 \\ 0 & 0 & 0 & 1 & 0 & 0 & 0 & 0 \\ 0 & 0 & 0 & 0 & 0 & 0 & 0 & \alpha \\ 0 & 0 & 0 & 0 & 0 & 1 & 0 & 0 \\ 0 & 0 & 0 & 0 & 0 & 0 & 1 & 0 \\ 0 & 0 & 0 & 0 & 0 & 0 & 0 & 1 \\ 0 & 0 & 0 & -\alpha & 0 & 0 & 0 & 0 \end{pmatrix}}_{\mathbf{A}} \mathbf{z}(x), \quad (1.26)$$

where

$$\mathbf{z}^\top(x) = \left(w(x) \quad \frac{\partial w(x)}{\partial x} \quad \frac{\partial^2 w(x)}{\partial x^2} \quad \frac{\partial^3 w(x)}{\partial x^3} \quad v(x) \quad \frac{\partial v(x)}{\partial x} \quad \frac{\partial^2 v(x)}{\partial x^2} \quad \frac{\partial^3 v(x)}{\partial x^3} \right).$$

The geometrical and the algebraic multiplicity of the eigenvalues of \mathbf{A} are different. Consequently, the general solution can be calculated by using the eigenvalues and eigenvectors of matrix \mathbf{A} of Eq. (1.26) but we have to take into account the generalized eigenvectors, too. The form of the general solution is

$$\begin{aligned} v(x) &= A + Bx + C \frac{x^2}{2} - K \sin(\alpha x) + N \cos(\alpha x), \\ w(x) &= D + Gx + H \frac{x^2}{2} + K \cos(\alpha x) + N \sin(\alpha x). \end{aligned} \quad (1.27)$$

Considering the boundary conditions Eq. (1.25), the system of equations assumes the form

$$\begin{pmatrix} 1 & 0 & 0 & 0 & 0 & 0 & 0 & 0 \\ 0 & 1 & 0 & 0 & 0 & 0 & 0 & 0 \\ 0 & 0 & 1 & 0 & 0 & 0 & 0 & 0 \\ 0 & 0 & 0 & 0 & 0 & 0 & 0 & 0 \\ 0 & 0 & 0 & 1 & 0 & 0 & 0 & 0 \\ 0 & 0 & 0 & 0 & 1 & 0 & 0 & 0 \\ 0 & 0 & 0 & 0 & 0 & 1 & 0 & 0 \\ 0 & 0 & 0 & 0 & 0 & 0 & 1 & 0 \end{pmatrix} \begin{pmatrix} 0 \\ -\alpha \\ \alpha^2 \sin(\alpha L) \\ \cos(\alpha L) \\ 1 \\ 0 \\ -\alpha^2 \cos(\alpha L) \\ \sin(\alpha L) \end{pmatrix} \begin{pmatrix} 1 \\ 0 \\ -\alpha^2 \cos(\alpha L) \\ \sin(\alpha L) \\ 0 \\ \alpha \\ -\alpha^2 \sin(\alpha L) \\ -\cos(\alpha L) \end{pmatrix} = \begin{pmatrix} A \\ B \\ C \\ D \\ G \\ H \\ K \\ N \end{pmatrix} = \begin{pmatrix} 0 \\ 0 \\ 0 \\ 0 \\ 0 \\ 0 \\ 0 \\ 0 \end{pmatrix}. \quad (1.28)$$

The determinant of the coefficient matrix is 1, that is, there is no critical value for M_t and only the stable trivial solution exists.

Case 2: This solution corresponds to the second order differential equation system of Eq. (1.24) and reduces the number of the boundary conditions.

The first step is to transform the original system of equations and consider its form

$$\begin{aligned} \frac{\partial}{\partial x} \underbrace{\left(\frac{\partial v(x)}{\partial x} + \alpha w(x) \right)}_{=a} &= 0, \\ \frac{\partial}{\partial x} \underbrace{\left(\frac{\partial w(x)}{\partial x} - \alpha v(x) \right)}_{=b} &= 0 \end{aligned} \quad (1.29)$$

where a and b must be constants, that is

$$\frac{\partial v(x)}{\partial x} + \alpha w(x) = C_1, \quad \frac{\partial w(x)}{\partial x} - \alpha v(x) = C_2. \quad (1.30)$$

Furthermore, the corresponding fixed end conditions Eq. (1.25) imply that C_1 and C_2 are both zero. Hence

$$\frac{\partial v(x)}{\partial x} = -\alpha w(x), \quad \frac{\partial w(x)}{\partial x} = \alpha v(x), \quad \forall x \in [0, L]. \quad (1.31)$$

Based on Eq. (1.31), the following expression can be obtained

$$\frac{\partial^2 w(x)}{\partial x^2} + \alpha^2 w(x) = 0 \quad (1.32)$$

that leads to the general solutions

$$w(x) = A \cos(\alpha x) + B \sin(\alpha x) \quad \Leftrightarrow \quad v(x) = -A \sin(\alpha x) + B \cos(\alpha x).$$

If we differentiate Eq. (1.31) twice with respect to x , then we can see that the boundary condition of the third derivative of $v(x)$ at $x = L$ implies the condition of the second derivative of $w(x)$ at $x = L$. The situation is the same at the other equation, too. So we could reduce the number of conditions from 8 to 6. The system of equations using these conditions is

$$\begin{pmatrix} \cos(\alpha L) & \sin(\alpha L) \\ \sin(\alpha L) & -\cos(\alpha L) \end{pmatrix} \begin{pmatrix} A \\ B \end{pmatrix} = \begin{pmatrix} 0 \\ 0 \end{pmatrix}. \quad (1.33)$$

The determinant of the coefficient matrix is 1, so there is no critical value for M_t , which means, we arrive back to the same solution as with the equilibrium approach Case 1 above.

The problem using kinetic approach (see Subsec. 1.1.1) was investigated by Troesch [28], it turned out that the beam buckles under an arbitrary small torque. The answer supplied by the kinetic approach is as wrong as the one

that was achieved by the equilibrium approach, that is, when the beam is unconditionally stable under an arbitrary torsional torque. Therefore, we need to investigate how the torsion is transmitted to the beam. One of the possible ways has been already introduced in Subsec. 1.1.2, namely, semi-tangential torsion.

1.2.4 Buckling by semi-tangential Torsion

Since the result shows that a cantilever beam under axial torsion is unconditionally stable, it is reasonable to investigate the same problem by using the semi-tangential torsion defined in Subsec. 1.1.2. The question is whether the beam becomes unstable under a corresponding torque or not. By using the equilibrium approach, the governing equations have two additional terms compared to Eq. (1.24) due to Eq. (1.9). So we obtain

$$\begin{aligned}\frac{\partial^2 v(x)}{\partial x^2} + \alpha \frac{\partial w(x)}{\partial x} &= \frac{1}{2} \alpha \delta'_w, \\ \frac{\partial^2 w(x)}{\partial x^2} - \alpha \frac{\partial v(x)}{\partial x} &= -\frac{1}{2} \alpha \delta'_v.\end{aligned}\tag{1.34}$$

For the sake of simplicity, let us introduce a complex function

$$d(x) = v(x) + iw(x).\tag{1.35}$$

If it is substituted into Eq. (1.34) and the simplifications are performed, we obtain

$$\frac{\partial^2 d(x)}{\partial x^2} - i\alpha \frac{\partial d(x)}{\partial x} = -\frac{1}{2} i\alpha d'_L, \quad d'_L = (\delta'_v + i\delta'_w).\tag{1.36}$$

The solution needs to be separated to a homogeneous part and a non-homogeneous part. Assuming the test function $d(x) = Ke^{\lambda x}$, the form of the homogeneous part is

$$\underbrace{Ke^{\lambda x}}_{\neq 0} (\lambda^2 - i\alpha\lambda) = 0\tag{1.37}$$

where

$$\lambda_1 = 0, \quad \lambda_2 = i\alpha \quad \Rightarrow \quad d_H(x) = A + Be^{\lambda_2 x}.\tag{1.38}$$

The non-homogeneous part is purely linear, so the general solution is

$$d(x) = A + Be^{\lambda_2 x} + \frac{1}{2} d'_L x.\tag{1.39}$$

Basically, we have four boundary conditions for the fixed end of the beam that can be reduced to two based on Eq. (1.35). We can also define two

boundary conditions for the free end of the beam. These conditions and terms are considered as

$$d(0) = \frac{\partial d(x)}{\partial x} \Big|_{x=0} = 0, \quad \text{and} \quad \frac{\partial d(x)}{\partial x} \Big|_{x=L} = d'_L. \quad (1.40)$$

To proceed, let us use the boundary conditions above for creating the system matrix of equations where we also consider d'_L as an unknown term:

$$\underbrace{\begin{pmatrix} 1 & 1 & 0 \\ 0 & \lambda_2 & \frac{1}{2} \\ 0 & \lambda_2 e^{\lambda_2 L} & -\frac{1}{2} \end{pmatrix}}_{=\mathbf{A}} \begin{pmatrix} A \\ B \\ d'_L \end{pmatrix} = \begin{pmatrix} 0 \\ 0 \\ 0 \end{pmatrix}. \quad (1.41)$$

The non-trivial solution of Eq. (1.41) is when the determinant of the system matrix vanishes:

$$-\frac{1}{2}\lambda_2(1 + e^{\lambda_2 L}) = 0, \quad (1.42)$$

that is true when $-1 = e^{\lambda_2 L}$. It implies

$$\left. \begin{array}{l} -1 = \cos(\alpha L) \\ 0 = \sin(\alpha L) \end{array} \right\} \alpha = (2n + 1)\frac{\pi}{L}, \quad n = 0, 1, \dots \quad (1.43)$$

So the first critical twisting torque ($n = 0$) is

$$M_t = \frac{\pi}{L} IE. \quad (1.44)$$

This cannot be found by using purely the axial torsion above, because the bending moment components originated in the semi-tangential moments are not taken into account there [30].

1.2.5 Buckling by axial Torsion and Compression

The goal of this section is to understand how a cantilever beam behaves under combined loads namely, under axial torsion and compression. According to the previous results, a straight cantilever beam might buckle under compression greater loading than Eq. (1.19). In case of axial torsion, there is no critical value based on the equilibrium approach for cantilever beams, while

critical value of torsion exists for a pinned-pinned beam as shown in literature [3]. By using Eqs. (1.6) and (1.7) considering $M_{y,z} = 0$ and $Q_{y,z} = 0$, we obtain

$$\begin{aligned}\frac{\partial^2 v(x)}{\partial x^2} + \alpha \frac{\partial w(x)}{\partial x} + \gamma v(x) &= \gamma \delta_v, \\ \frac{\partial^2 w(x)}{\partial x^2} - \alpha \frac{\partial v(x)}{\partial x} + \gamma w(x) &= \gamma \delta_w.\end{aligned}\tag{1.45}$$

Similarly to the Subsec. 1.2.4, the introduced complex function is able to simplify our system:

$$\frac{\partial^2 d(x)}{\partial x^2} - i\alpha \frac{\partial d(x)}{\partial x} + \gamma d(x) = \gamma d_L, \quad d_L = (\delta_v + i\delta_w).\tag{1.46}$$

Assuming the same test function, the homogeneous part gives

$$\underbrace{K e^{\lambda x}}_{\neq 0} (\lambda^2 - i\alpha\lambda + \gamma) = 0\tag{1.47}$$

where

$$\lambda_{1,2} = \frac{\alpha \pm \sqrt{\alpha^2 + 4\gamma}}{2} i \Rightarrow d_H(x) = A e^{\lambda_1 x} + B e^{\lambda_2 x}.\tag{1.48}$$

Since the non-homogeneous part of the differential equation is constant, the general solution assumes the form

$$d(x) = A e^{\lambda_1 x} + B e^{\lambda_2 x} + d_L.\tag{1.49}$$

The boundary conditions and the defined term for the end of the beam are given by

$$d(0) = \left. \frac{\partial d(x)}{\partial x} \right|_{x=0} = 0, \quad \text{and} \quad d(L) = d_L.\tag{1.50}$$

These are used to create the system matrix of equations:

$$\underbrace{\begin{pmatrix} 1 & 1 & 1 \\ \lambda_1 & \lambda_2 & 0 \\ e^{\lambda_1 L} & e^{\lambda_2 L} & 0 \end{pmatrix}}_{=\mathbf{A}} \begin{pmatrix} A \\ B \\ d_L \end{pmatrix} = \begin{pmatrix} 0 \\ 0 \\ 0 \end{pmatrix}.\tag{1.51}$$

The non-trivial solution of Eq. (1.51) is

$$\lambda_1 e^{\lambda_2 L} - \lambda_2 e^{\lambda_1 L} = 0,\tag{1.52}$$

that can be transformed to the form

$$\frac{\lambda_1}{\lambda_2} = e^{(\lambda_1 - \lambda_2)L}. \quad (1.53)$$

If we introduce the notation of $\lambda_{1,2} = k_{1,2}i$ and use the Euler-formula, Eq. (1.53) gives

$$\begin{aligned} \frac{k_1}{k_2} &= \cos((k_1 - k_2)L), \\ 0 &= \sin((k_1 - k_2)L). \end{aligned} \quad (1.54)$$

The addition of the equations of (1.54) gives rise to $k_1^2 \neq k_2^2$, that is, there does not exist critical value of the applied loads in this configuration. When the effect of torsion ceases, that is, $\alpha = 0$, we arrive back to the critical load of compression.

1.2.6 Buckling by axial Torsion and Tension

Subsec. 1.2.5 discovered that the assumption of buckling occurs under axial torsion and compression using equilibrium approach is not correct. We could not find any critical values of the combined load. The steps of the solution are also the same at tension, that is, it can be figured out that there are no critical values at a twisted and tensed cantilever beam neither. So the cantilever beam is unconditionally stable again such as in case of only axial torsion (see Subsec. 1.2.3).

1.2.7 Buckling by semi-tangential Torsion and Compression

The equilibrium approach by using axial torque did not satisfy the assumption that claims: a twisted and compressed cantilever beam might buckle, so we need to investigate the same structure under semi-tangential torsion. The complex differential equation to be analysed must be a compound of Eqs. (1.36) and (1.46), that is

$$\frac{\partial^2 d(x)}{\partial x^2} - i\alpha \frac{\partial d(x)}{\partial x} + \gamma d(x) = \gamma d_L - \frac{1}{2}i\alpha d'_L. \quad (1.55)$$

The homogeneous solution of Eq. (1.55) corresponds to the Eq. (1.48). Since the non-homogeneity is purely a constant number, the non-homogeneous solution will also be constant. Therefore, the general solution of Eq. (1.55) assumes the form

$$d(x) = Ae^{\lambda_1 x} + Be^{\lambda_2 x} + d_L - \frac{\alpha}{2\gamma} i d'_L. \quad (1.56)$$

By using the boundary conditions defined by Eqs. (1.40) and (1.50), we obtain

$$\underbrace{\begin{pmatrix} 1 & 1 & 1 & -\frac{\alpha}{2\gamma}i \\ \lambda_1 & \lambda_2 & 0 & 0 \\ e^{\lambda_1 L} & e^{\lambda_2 L} & 0 & -\frac{\alpha}{2\gamma}i \\ \lambda_1 e^{\lambda_1 L} & \lambda_2 e^{\lambda_2 L} & 0 & -1 \end{pmatrix}}_{=\mathbf{A}} \begin{pmatrix} A \\ B \\ d_L \\ d'_L \end{pmatrix} = \begin{pmatrix} 0 \\ 0 \\ 0 \\ 0 \end{pmatrix}. \quad (1.57)$$

The non-trivial solution of Eq. (1.57) is

$$\cos\left(\frac{\sqrt{\alpha^2 + 4\gamma}L}{2}\right) = 0 \quad (1.58)$$

that implies

$$\alpha^2 + 4\gamma = (2n + 1)^2 \left(\frac{\pi}{L}\right)^2 \quad n = 0, 1, \dots, \quad (1.59)$$

where n is an integer. If we multiply Eq. (1.59) by $(L/\pi)^2$, then it yields

$$\underbrace{\left(\frac{\alpha L}{\pi}\right)^2}_{=m_t^2} + \underbrace{\frac{4\gamma L^2}{\pi^2}}_{=p} = (2n + 1)^2 \Rightarrow m_t^2 + p = (2n + 1)^2, \quad (1.60)$$

where parameter m_t represents the relative importance of torsion to the first critical value of semi-tangential torsion and p represents the relative importance of compression to the first critical value of compression.

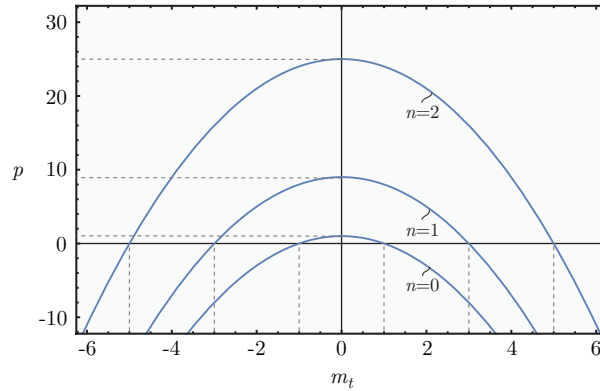


Figure 1.4: Dimensionless stability diagram of semi-tangential torsion and compression/tension.

The relationship between m_t and p is parabolic meaning that the increasing value of torsion decreases the value of compression and vice versa (see Fig. 1.4). Note that the curves are crossing the axis m_t at the normalized critical values of the semi-tangential torque and crossing the axis p at the normalized Euler critical buckling loads [30].

1.2.8 Buckling by semi-tangential Torsion and Tension

As we know, a tensed cantilever beam has no critical case in sense of structural stability. This can also be explained by the stiffness variation of the system. While compression decreases the stiffness of the system, tension increases that. The issue is whether this effect could be influenced by a twisting moment. The way of calculation in accordance with Subsec. 1.2.7's, the only difference is the negative sign of γ .

The stability boundaries for a twisted and tensed beam can also be seen in Fig. 1.4 because $p < 0$ describes the case of tension. Accordingly, we can see that tension is able to delay the effect of torsion (see Fig. 1.4).

1.3 Deformation functions

To support the extended dynamical modelling, it is necessary to investigate how the cantilever beam deforms under combined loads. Basically, we need to consider the global system in Fig. 1.2, where we take into account the lateral forces and bending moments at the free end of the beam. Based on the deformation functions v and w , we are able to analyse the displacements of the free end of the beam. It will be useful to define either an equivalent lateral spring stiffness or a corresponding compliance matrix.

1.3.1 Compressed beam

To determine the deformation function, we have to utilize the differential equation (1.6) considering $M_t = 0$, which yields

$$\frac{\partial^2 v(x)}{\partial x^2} + \gamma v(x) = \gamma \delta_v + \frac{Q_y}{IE}(L - x) + \frac{M_z}{IE}. \quad (1.61)$$

Again, the solution of Eq. (1.61) consists of a homogeneous part and a particular part. Assuming the test function $v(x) = Ke^{\lambda x}$, we obtain

$$\underbrace{Ke^{\lambda x}}_{\neq 0}(\lambda^2 + \gamma) = 0 \quad \Rightarrow \quad \lambda_{1,2} = \pm\sqrt{\gamma}i. \quad (1.62)$$

In this case, the non-homogeneous part is purely linear, thus the shape of the particular solution function is $v_P(x) = Cx + D$. If it is substituted into Eq. (1.61) and we calculate the unknown coefficients C and D , the general solution is given by

$$v(x) = A \cos(\sqrt{\gamma}x) + B \sin(\sqrt{\gamma}x) - \frac{1}{\gamma IE} (Q_y(x - L) - M_z) + \delta_v. \quad (1.63)$$

The boundary conditions correspond to Eq. (1.20), which leads to the linear non-homogeneous matrix equation

$$\underbrace{\begin{pmatrix} 1 & 0 & 1 \\ 0 & \sqrt{\gamma} & 0 \\ \cos(\sqrt{\gamma}L) & \sin(\sqrt{\gamma}L) & 0 \end{pmatrix}}_{=\mathbf{A}} \begin{pmatrix} A \\ B \\ \delta_v \end{pmatrix} = \underbrace{\begin{pmatrix} -\frac{1}{\gamma IE} (Q_y L + M_z) \\ \frac{Q_y}{\gamma IE} \\ -\frac{M_z}{\gamma IE} \end{pmatrix}}_{=\mathbf{B}}. \quad (1.64)$$

The coefficient vector can be determined by the expression of $\mathbf{A}^{-1}\mathbf{B}$ that gives the specific solution

$$\begin{aligned} v(x) = & -\frac{1}{\gamma IE} \left(\frac{M_z}{\cos(\sqrt{\gamma}L)} + \frac{Q_y \tan(\sqrt{\gamma}L)}{\sqrt{\gamma}} \right) \cos(\sqrt{\gamma}x) \\ & + \frac{Q_y}{\gamma \sqrt{\gamma} IE} \sin(\sqrt{\gamma}x) - \frac{1}{\gamma IE} (Q_y(x - L) - M_z) \\ & + \frac{M_z \sqrt{\gamma} \left(\frac{1}{\cos(\sqrt{\gamma}L)} - 1 \right) + Q_y (\tan(\sqrt{\gamma}L) - L \sqrt{\gamma})}{\gamma \sqrt{\gamma} IE}. \end{aligned} \quad (1.65)$$

Since we are going to investigate the displacements of the end of the beam, it is reasonable to provide the value of the function v at $x = L$

$$v(L) = \frac{M_z \sqrt{\gamma} \left(\frac{1}{\cos(\sqrt{\gamma}L)} - 1 \right) + Q_y (\tan(\sqrt{\gamma}L) - L \sqrt{\gamma})}{\gamma \sqrt{\gamma} IE}, \quad (1.66)$$

that corresponds with the notation δ_v . When M_z tends to zero, the power series of Eq. (1.66) with respect to $L^2\gamma$ can be expressed by

$$\delta_v = \frac{Q_y L^3}{IE} \left(\frac{1}{3} + \frac{2}{15} (L^2\gamma) + \frac{17}{315} (L^2\gamma)^2 + \dots \right). \quad (1.67)$$

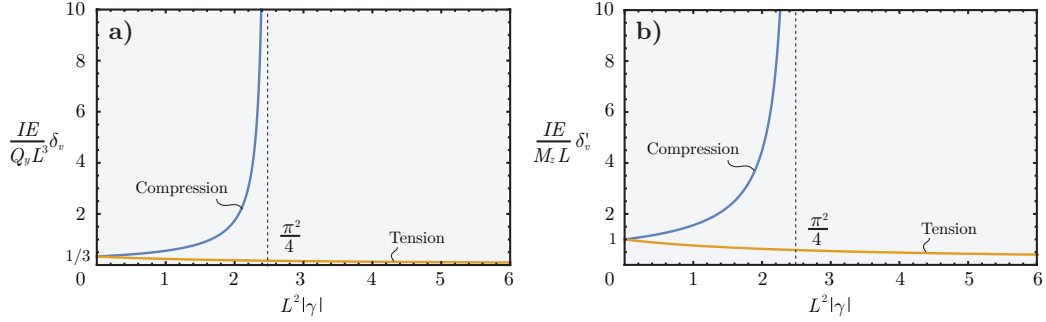


Figure 1.5: a) Dimensionless relationship between the relative importance of compression/tension and the relative importance of the displacement of the end of the beam. b) Dimensionless relationship between the relative importance of compression/tension and the relative importance of the angular rotation of the end of the beam. $L^2\gamma = (2n + 1)^2(\pi/2)^2$ - where $n = 0, 1, 2, \dots$ - is proportional to the critical load of compression (see Eq. (1.19)).

When Q_y tends to zero, the power series of the first derivative of Eq. (1.65) is given by

$$\delta'_v = \frac{M_z L}{IE} \left(1 + \frac{1}{3} (L^2 \gamma) + \frac{2}{15} (L^2 \gamma)^2 + \dots \right). \quad (1.68)$$

The power series are depicted in Fig. 1.5 that shows how the relative displacement and angular rotation change with respect to dimensionless compression.

1.3.2 Beam in Tension

Similarly to Subsec. 1.3.1, the general solution of the observed tensed beam can be expressed as

$$v(x) = A \cosh(\sqrt{\gamma}x) + B \sinh(\sqrt{\gamma}x) - \frac{1}{\gamma IE} (Q_y(L - x) + M_z) + \delta_v. \quad (1.69)$$

The boundary conditions also correspond to Eq. (1.20), so the system of the equations is

$$\begin{pmatrix} 1 & 0 & 1 \\ 0 & \sqrt{\gamma} & 0 \\ \cosh(\sqrt{\gamma}L) & \sinh(\sqrt{\gamma}L) & 0 \end{pmatrix} \begin{pmatrix} A \\ B \\ \delta_v \end{pmatrix} = \begin{pmatrix} \frac{1}{\gamma IE} (Q_y L + M_z) \\ -\frac{Q_y}{\gamma IE} \\ \frac{M_z}{\gamma IE} \end{pmatrix}. \quad (1.70)$$

Therefore, the deformation function is

$$\begin{aligned}
 v(x) = & \frac{1}{\gamma IE} \left(\frac{M_z}{\cosh(\sqrt{\gamma}L)} + \frac{Q_y \tanh(\sqrt{\gamma}L)}{\sqrt{\gamma}} \right) \cosh(\sqrt{\gamma}x) \\
 & - \frac{Q_y}{\gamma\sqrt{\gamma}IE} \sinh(\sqrt{\gamma}x) - \frac{1}{\gamma IE} (Q_y(L-x) + M_z) \\
 & + \frac{M_z\sqrt{\gamma} \left(1 - \frac{1}{\cosh(\sqrt{\gamma}L)} \right) + Q_y (L\sqrt{\gamma} - \tanh(\sqrt{\gamma}L))}{\gamma\sqrt{\gamma}IE}.
 \end{aligned} \tag{1.71}$$

The displacement of the end of the beam also equals with δ_v , that is

$$v(L) = \frac{M_z\sqrt{\gamma} \left(1 - \frac{1}{\cosh(\sqrt{\gamma}L)} \right) + Q_y (L\sqrt{\gamma} - \tanh(\sqrt{\gamma}L))}{\gamma\sqrt{\gamma}IE}. \tag{1.72}$$

When M_z tends to zero, the power series of Eq. (1.72) is given by

$$\delta_v = \frac{Q_y L^3}{IE} \left(\frac{1}{3} - \frac{2}{15} (L^2\gamma) + \frac{17}{315} (L^2\gamma)^2 \mp \dots \right). \tag{1.73}$$

When Q_y tends to zero, the power series of the first derivative of Eq. (1.71) can be expressed by

$$\delta'_v = \frac{M_z L}{IE} \left(1 - \frac{1}{3} (L^2\gamma) + \frac{2}{15} (L^2\gamma)^2 \mp \dots \right). \tag{1.74}$$

The power series are depicted in Fig. 1.5 that shows how the relative displacement and angular rotation change with respect to dimensionless tension.

1.3.3 Beam subjected to axial Torsion

Let us consider a cantilever beam subjected to axial torsion, lateral forces and bending moments at its free end, that is, using Eqs. (1.6) and (1.7) where we assume that $P = 0$:

$$\begin{aligned}
 \frac{\partial^2 v(x)}{\partial x^2} + \alpha \frac{\partial w(x)}{\partial x} &= \frac{Q_y}{IE} (L-x) + \frac{M_z}{IE}, \\
 \frac{\partial^2 w(x)}{\partial x^2} - \alpha \frac{\partial v(x)}{\partial x} &= \frac{Q_z}{IE} (L-x) - \frac{M_y}{IE}.
 \end{aligned} \tag{1.75}$$

According to the previously defined complex function d (see Eq. (1.35)), Eq. (1.75) assumes the form

$$\frac{\partial^2 d(x)}{\partial x^2} - i\alpha \frac{\partial d(x)}{\partial x} = \Gamma + \Lambda(L - x), \quad (1.76)$$

where

$$\Gamma = \frac{1}{IE}(M_z - iM_y), \quad \Lambda = \frac{1}{IE}(Q_y + iQ_z).$$

The linear, non-homogeneous, complex differential equation is needed to give a homogeneous solution that can be simply calculated as

$$d_H(x) = A + Be^{i\alpha x}. \quad (1.77)$$

The test function of the particular solution is second order $d_P(x) = Cx^2 + Dx$, where C , D are constant coefficients. The superposition of the homogeneous solution and the particular solution gives the complex deformation function of the beam

$$\begin{aligned} d(x) &= d_H(x) + d_P(x) \\ &= A + Be^{i\alpha x} + \frac{\Lambda}{2i\alpha}x^2 + \frac{i}{\alpha} \left((\Gamma + \Lambda L) + \frac{\Lambda i}{\alpha} \right) x. \end{aligned} \quad (1.78)$$

In order to proceed, it is necessary to have two boundary conditions that refer to the fixed end of the beam

$$d(0) = \left. \frac{\partial d(x)}{\partial x} \right|_{x=0} = 0. \quad (1.79)$$

By using the introduced boundary conditions, we are able to calculate the unknown coefficients A , B . Hence the complex deformation function is

$$d(x) = \frac{1}{\alpha} \left(\frac{\Lambda i}{\alpha} + (\Gamma + \Lambda L) \right) \left(\frac{1}{\alpha} (1 - e^{i\alpha x}) + ix \right) - \frac{\Lambda i}{2\alpha} x^2. \quad (1.80)$$

Considering (1.80) at $x = L$, it yields that we investigate the end point of the beam, where $d(L)$ is denoted by d_L and $d'(L)$ is denoted by d'_L . When Γ tends to zero, the power series of Eq. (1.80) with respect to $iL\alpha$ is

$$d_L = L^3 \Lambda \left(\frac{1}{3} + \frac{1}{8}(iL\alpha) + \frac{1}{30}(iL\alpha)^2 + \dots \right). \quad (1.81)$$

When Λ tends to zero, the power series of the first derivative of Eq. (1.80) is given by

$$d'_L = L\Gamma \left(1 + \frac{1}{2}(iL\alpha) + \frac{1}{6}(iL\alpha)^2 + \dots \right). \quad (1.82)$$

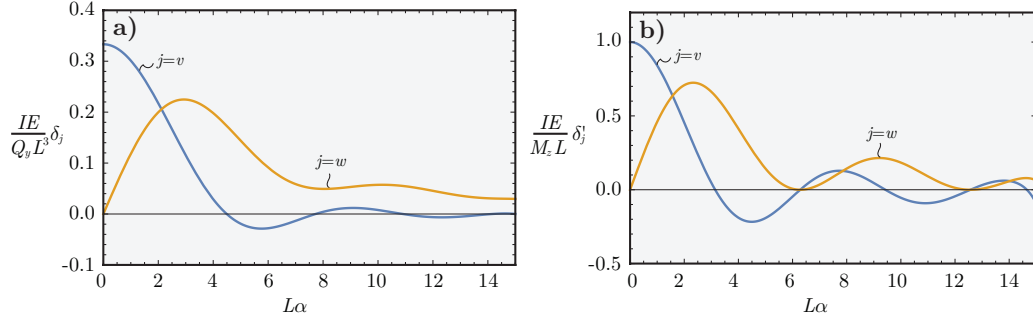


Figure 1.6: a) Dimensionless relationship between the relative importance of axial torsion and the relative importance of the displacement of the end of the beam ($Q_z = 0$, $M_{y,z} = 0$). b) Dimensionless relationship between the relative importance of axial torsion and the relative importance of the angular rotation of the end of the beam ($Q_{y,z} = 0$, $M_y = 0$).

Eq. (1.80) can be separated to the real part and the imaginary part. The definition of the complex function d provides that $\delta_v = \text{Re}(d(L))$ and $\delta_w = \text{Im}(d(L))$, so

$$\delta_v = \frac{1}{\alpha^2} \left(M_z + \frac{Q_y \sin(\alpha L)}{\alpha} - \cos(\alpha L)(M_z + Q_y L) \right) \quad (1.83)$$

and

$$\delta_w = \frac{1}{\alpha} \left(M_z L + Q_y \left(\frac{1 - \cos(\alpha L)}{\alpha^2} + \frac{L^2}{2} \right) - \frac{\sin(\alpha L)}{\alpha} (M_z + Q_y L) \right), \quad (1.84)$$

where Q_z and M_y are zero. The resolution of the complex function $d'(L)$ can be similarly calculated where $\delta'_v = \text{Re}(d'(L))$ and $\delta'_w = \text{Im}(d'(L))$. $\delta_{v,w}$ and $\delta'_{v,w}$ are depicted in Fig. 1.6. Based on Eqs. (1.81) and (1.82), when $Q_y = Q_z$ and $M_y = M_z$, the dimensionless displacement and angular rotation maps can be seen in Fig. 1.7. It can be observed that, for example, the applied lateral forces $Q_{y,z}$ and the displacement d_L of the end of the beam are bidirectional (see Eqs. (1.81) again). By taking into account the first term of the power series, we can see that Λ is proportional to the lateral forces, hence why the first term is evidently equidirectional to d_L . The second term in the presence of the axial torsion α destroys this feature and makes this relation bidirectional [30], that is, the displacement d_L will not have the direction of the lateral force. This can be seen also in case of the bending moments $M_{y,z}$.

Note that when we increase the axial torsional moment, the end of the beam follows a spiral orbit. When either the lateral forces $Q_{y,z}$ or the bending

moments $M_{y,z}$ are zero, we obtain again the previous stability problem (see Subsec. 1.2.3), namely, there is no non-trivial equilibrium configuration. Now the result is even more general: the axial torsion does not lead to instability even in the presence of any lateral forces $Q_{y,z}$ and/or bending moments $M_{y,z}$.

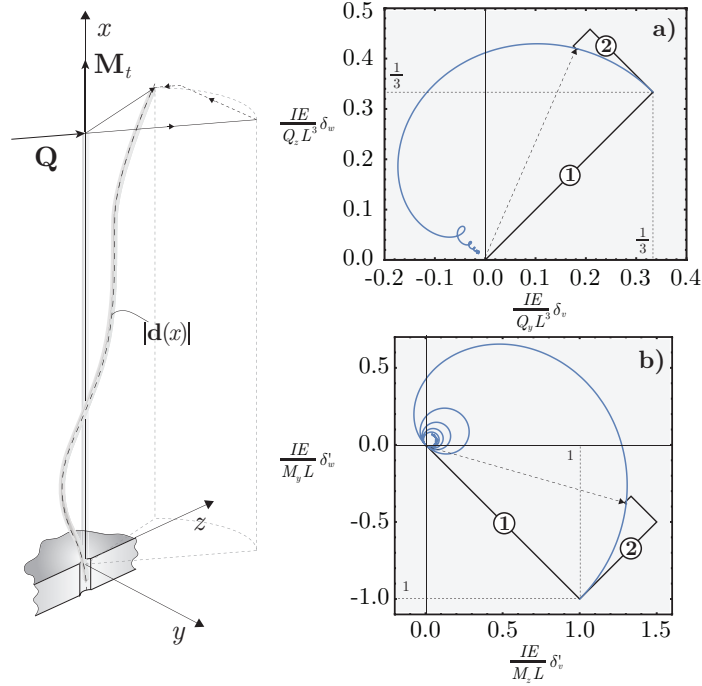


Figure 1.7: Displacement/angular rotation of the end of the beam where $\mathbf{d} = \text{col}(v \ w)$ and $\mathbf{Q} = \text{col}(Q_y \ Q_z)$. a) Dimensionless relationship in between the relative importance of displacements when $M_{y,z} = 0$. b) Dimensionless relationship in between the relative importance of angular rotations when $Q_{y,z} = 0$. Here, the circled numbers mean the corresponding terms of the power series of Eqs. (1.81) and (1.82).

1.3.4 Beam subjected to semi-tangential Torsion

To resolve the above incorrect stability result related to axial torsion in Subsec. 1.3.3, we need to take into account Eq. 1.9 that considers the additional terms of semi-tangential torque. Thus the governing equations assume the form

$$\begin{aligned} \frac{\partial^2 v(x)}{\partial x^2} + \alpha \frac{\partial w(x)}{\partial x} &= \frac{Q_y}{IE}(L-x) + \frac{M_z}{IE} + \frac{1}{2}\alpha\delta'_w, \\ \frac{\partial^2 w(x)}{\partial x^2} - \alpha \frac{\partial v(x)}{\partial x} &= \frac{Q_z}{IE}(L-x) - \frac{M_y}{IE} - \frac{1}{2}\alpha\delta'_v. \end{aligned} \quad (1.85)$$

Again, by using the complex displacement function d , we obtain a complex differential equation

$$\frac{\partial^2 d(x)}{\partial x^2} - i\alpha \frac{\partial d(x)}{\partial x} = \Gamma + \Lambda(L - x) - \frac{1}{2}i\alpha d'_L. \quad (1.86)$$

The general solution can be calculated similarly to Eq. (1.78), so we obtain

$$\begin{aligned} d(x) &= d_H(x) + d_P(x) \\ &= A + Be^{i\alpha x} + \frac{\Lambda}{2i\alpha}x^2 + \left(\frac{i}{\alpha} \left((\Gamma + \Lambda L) + \frac{\Lambda i}{\alpha} \right) + \frac{1}{2}d'_L \right) x. \end{aligned} \quad (1.87)$$

In this case, we need to have two boundary conditions and a definition that refers to the rotation angles at the free end of the beam:

$$d(0) = \frac{\partial d(x)}{\partial x} \Big|_{x=0} = 0, \quad \text{and} \quad \frac{\partial d(x)}{\partial x} \Big|_{x=L} = d'_L. \quad (1.88)$$

By means of the boundary conditions, the unknown coefficients A , B can be calculated

$$\begin{aligned} d(x) &= \frac{i}{\alpha e^{i\alpha L}} \left(\frac{1}{2}d'_L + \frac{1}{i\alpha} \left(\frac{\Lambda i}{\alpha} + \Gamma \right) \right) (1 - e^{i\alpha x}) \\ &\quad + \frac{\Lambda}{2i\alpha}x^2 + \left(\frac{i}{\alpha} \left((\Gamma + \Lambda L) + \frac{\Lambda i}{\alpha} \right) + \frac{1}{2}d'_L \right) x, \end{aligned} \quad (1.89)$$

where

$$d'_L = \frac{2}{1 + e^{-i\alpha L}} \left(\frac{e^{-i\alpha L}}{i\alpha} \left(\frac{\Lambda}{i\alpha} - \Gamma \right) + \frac{1}{i\alpha} \left(\frac{\Lambda i}{\alpha} + (\Gamma + \Lambda L) \right) \right).$$

The exact value of the displacement of the end point of the beam is given by

$$d_L = \frac{iL}{\alpha^2}(\alpha\Gamma + i\Lambda) + \frac{1}{2\alpha^3}(L\alpha - 2i)(2(\alpha\Gamma + i\Lambda) + L\alpha\Lambda) \tan\left(\frac{\alpha L}{2}\right). \quad (1.90)$$

When Γ is zero, the power series of Eq. (1.90) with respect to $iL\alpha$ is

$$d_L = L^3\Lambda \left(\frac{1}{3} - \frac{7}{240}(iL\alpha)^2 + \frac{59}{20160}(iL\alpha)^4 \mp \dots \right). \quad (1.91)$$

When Q_z is zero, that is, $\Lambda = Q_y/IE$ then

$$d_L = \delta_v. \quad (1.92)$$

The power series shows how the displacement is changed by torsion. Basically, torsion increases the lateral displacement but in this case because of the dimensionless nature, the power series is influenced by the quantity of $iL\alpha$. Note that when $M_{y,z} = 0$, the lateral force and the displacement are unidirectional compared to the case of axial torsion.

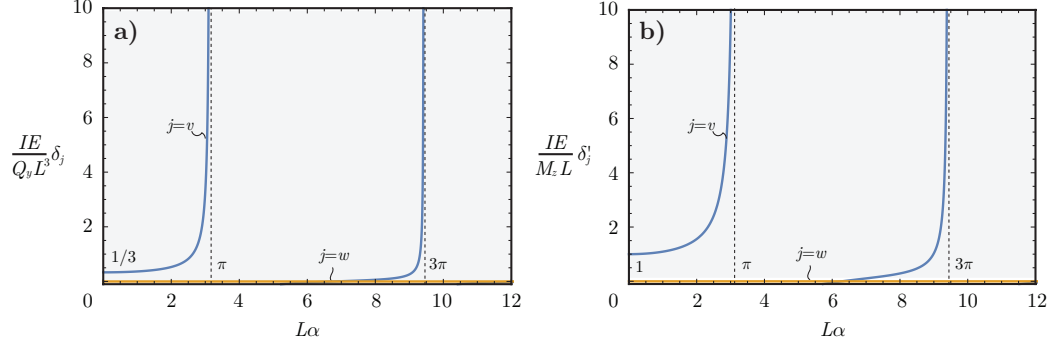


Figure 1.8: a) Dimensionless relationship between the relative importance of semi-tangential torsion and the relative importance of the displacement of the end of the beam ($Q_z = 0$, $M_{y,z} = 0$). b) Dimensionless relationship between the relative importance of semi-tangential torsion and the relative importance of the angular rotation of the end of the beam ($Q_{y,z} = 0$, $M_y = 0$). $L\alpha = (2n + 1)\pi$ - where $n = 0, 1, 2, \dots$ - is proportional to the critical load of semi-tangential torsion (see Eq. (1.44)).

1.3.5 Beam subjected to axial Torsion and Compression

In case of a boring, the bar is also affected by compression, thus we have to examine a twisted and compressed cantilever beam. The system is described by Eqs. (1.6) and (1.7):

$$\begin{aligned} \frac{\partial^2 v(x)}{\partial x^2} + \alpha \frac{\partial w(x)}{\partial x} + \gamma v(x) &= \gamma \delta_v + \frac{Q_y}{IE}(L - x) + \frac{M_z}{IE}, \\ \frac{\partial^2 w(x)}{\partial x^2} - \alpha \frac{\partial v(x)}{\partial x} + \gamma w(x) &= \gamma \delta_w + \frac{Q_z}{IE}(L - x) - \frac{M_y}{IE}. \end{aligned} \quad (1.93)$$

For the sake of simplicity, let us use the complex function d again, that gives

$$\frac{\partial^2 d(x)}{\partial x^2} - i\alpha \frac{\partial d(x)}{\partial x} + \gamma d(x) = \gamma d_L + \Gamma + \Lambda(L - x). \quad (1.94)$$

By using the test function $d_H(x) = Ke^{\lambda x}$ to get the homogeneous solution, we obtain

$$Ke^{\lambda x}(\lambda^2 - i\alpha\lambda + \gamma) = 0 \quad \Rightarrow \quad \lambda_{1,2} = \frac{\alpha \pm \sqrt{\alpha^2 + 4\gamma}}{2}i. \quad (1.95)$$

To proceed, we need to introduce another test function $d_P(x) = Cx + D$ where C, D are unknown coefficients. Hence the general solution of the system is

$$\begin{aligned} d(x) &= d_H(x) + d_P(x) \\ &= Ae^{\lambda_1 x} + Be^{\lambda_2 x} - \frac{\Lambda}{\gamma}x + \frac{1}{\gamma} \left(\Gamma + \Lambda \left(L - \frac{i\alpha}{\gamma} \right) \right) + d_L. \end{aligned} \quad (1.96)$$

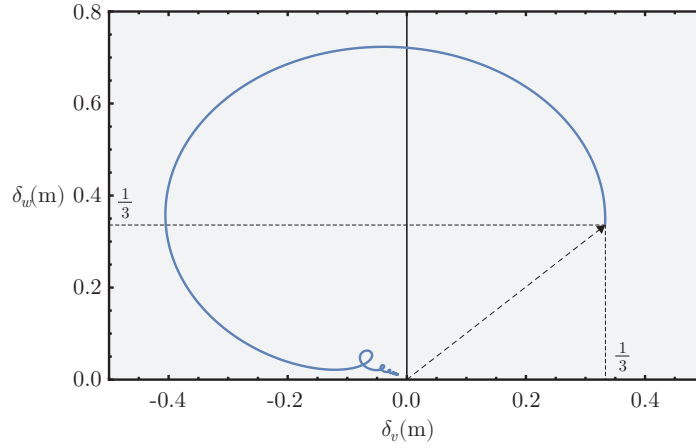


Figure 1.9: Numerical result for the displacement of the end of the beam by compression when $\Gamma = 0$ and where $L = 1$ (m), $|\mathbf{\Lambda}| = \sqrt{2}$ (m^{-2}) (Here, $\mathbf{\Lambda} = \text{col}(Q_y \ Q_z)/(IE)$), $\alpha = 0, 0.01, 0.02 \dots 40$ ($1/\text{m}$), $\gamma = 0, 0.01, 0.02 \dots 40$ (m^{-2}).

The following boundary conditions are needed

$$d(0) = \left. \frac{\partial d(x)}{\partial x} \right|_{x=0} = 0 \quad \text{and} \quad d(L) = d_L. \quad (1.97)$$

Based on the boundary conditions, the unknown coefficients A, B and d_L can be calculated. Note that the displacements and the lateral forces ($Q_{y,z}$) are bidirectional similarly to Subsec. 1.3.3. Fig. 1.9 shows a numerical result for the displacement variation of the end of the beam.

1.3.6 Beam subjected to semi-tangential Torsion and Compression

To investigate the problem by using the semi-tangential torque, we need to complete Eq. (1.94) with the terms of Eq. (1.9) which provide

$$\frac{\partial^2 d(x)}{\partial x^2} - i\alpha \frac{\partial d(x)}{\partial x} + \gamma d(x) = \gamma d_L + \Gamma + \Lambda(L - x) - \frac{1}{2}i\alpha d'_L. \quad (1.98)$$

The general solution can be expressed as

$$\begin{aligned} d(x) &= d_{\text{H}}(x) + d_{\text{P}}(x) \\ &= Ae^{\lambda_1 x} + Be^{\lambda_2 x} - \frac{\Lambda}{\gamma}x + \frac{1}{\gamma} \left(\Gamma + \Lambda \left(L - \frac{i\alpha}{\gamma} \right) \right) + d_L \boxed{-\frac{i\alpha}{2\gamma}d'_L}. \end{aligned} \quad (1.99)$$

The difference between axial torsion and semi-tangential torsion reveals only in the boxed term of Eq. (1.99). The unknown coefficients A , B , d_L and d'_L can be determined by using the boundary conditions

$$d(0) = \frac{\partial d(x)}{\partial x} \Big|_{x=0} = 0, \quad \text{and} \quad d(L) = d_L, \quad \frac{\partial d(x)}{\partial x} \Big|_{x=L} = d'_L. \quad (1.100)$$

If we assume that $Q_z = 0$ and $M_{y,z} = 0$, then the imaginary part of the complex deflection curve $d(x)$ defined by $w(x)$ ceases. It means that the applied lateral forces at the end of the beam and the displacements are unidirectional.

1.3.7 Beam subjected to axial Torsion and Tension

The problem corresponds to the case of Subsec. 1.3.5. The only difference appears in the sign of γ , that is, it works as tension. The governing differential equation is

$$\frac{\partial^2 d(x)}{\partial x^2} - i\alpha \frac{\partial d(x)}{\partial x} - \gamma d(x) = -\gamma d_L + \Gamma + \Lambda(L - x) \quad (1.101)$$

and its general solution can be expressed as

$$\begin{aligned} d(x) &= d_{\text{H}}(x) + d_{\text{P}}(x) \\ &= Ae^{\lambda_1 x} + Be^{\lambda_2 x} + \frac{\Lambda}{\gamma}x - \frac{1}{\gamma} \left(\Gamma + \Lambda \left(L + \frac{i\alpha}{\gamma} \right) \right) + d_L, \end{aligned} \quad (1.102)$$

where

$$\lambda_{1,2} = \frac{\alpha \pm \sqrt{\alpha^2 - 4\gamma}}{2} i.$$

The boundary conditions correspond to Eq. (1.97), hence why the unknown coefficients can be calculated. The presence of the bidirectional nature also gives rise to a bent orbit that can be seen in Fig. 1.10.

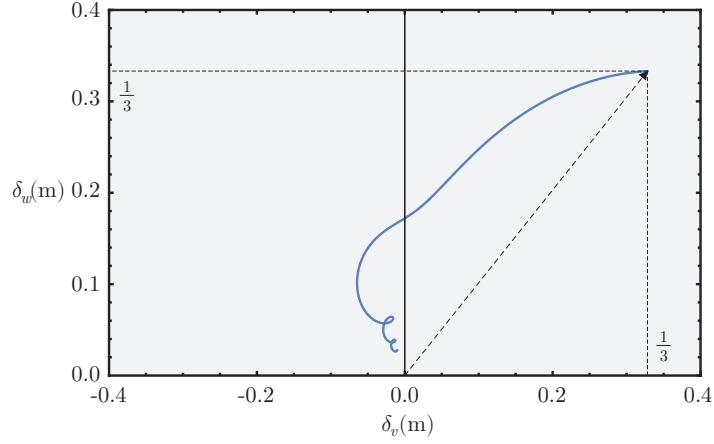


Figure 1.10: Numerical result for the displacement of the end of the beam by tension when $\Gamma = 0$ and where $L = 1$ (m), $|\mathbf{\Lambda}| = \sqrt{2}$ (m^{-2}) (Here, $\mathbf{\Lambda} = \text{col}(Q_y \ Q_z)/(IE)$), $\alpha = 0, 0.01, 0.02 \dots 12$ ($1/\text{m}$), $\gamma = 0, 0.01, 0.02 \dots 12$ (m^{-2}).

1.3.8 Beam subjected to semi-tangential Torsion and Tension

The problem is fairly similar to Subsec. 1.3.6 meaning that the only difference is the sign of γ in the equations. Therefore, the complex differential equation is

$$\frac{\partial^2 d(x)}{\partial x^2} - i\alpha \frac{\partial d(x)}{\partial x} - \gamma d(x) = -\gamma d_L + \Gamma + \Lambda(L - x) - \frac{1}{2}i\alpha d'_L \quad (1.103)$$

and its general solution is given by

$$\begin{aligned} d(x) &= d_H(x) + d_P(x) \\ &= Ae^{\lambda_1 x} + Be^{\lambda_2 x} + \frac{\Lambda}{\gamma}x - \frac{1}{\gamma} \left(\Gamma + \Lambda \left(L + \frac{i\alpha}{\gamma} \right) \right) + d_L + \frac{i\alpha}{2\gamma} d'_L \end{aligned} \quad (1.104)$$

where the form of $\lambda_{1,2}$ corresponds with the result of Subsec. 1.3.7. The boundary conditions do not change as compared to Subsec. 1.3.6 either. The unidirectional feature between the lateral forces and the displacement of the end of the beam can be simply proven here, too.

1.4 Displacement Analysis by Energy Approach

This section particularly deals with the case of compression but also provides close formulas for tension.

When a cantilever beam is subjected to both lateral force and compression or tension, the observed displacements of the end of the beam that affect the

natural frequencies of the system are not in agreement with the classical beam theory. The purpose of this section is to investigate these displacements in more details in order to provide a better approximation of the reality. Since the following problem is only two-dimensional, for the sake of simplicity, we are going to introduce some specific notation.

According to the results of Beléndez *et al.* [5], we are able to specify

$$\xi = \kappa \eta^2 \quad (1.105)$$

that describes the connection of the longitudinal displacement ξ and the lateral displacement η of a cantilever beam subjected to a lateral force Q_y at its free end (see Fig. 1.11 a)).

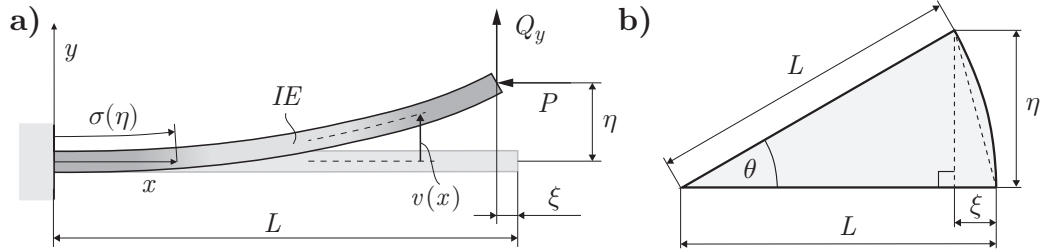


Figure 1.11: a) Model of the cantilever beam subjected to lateral force Q_y and compression P at its free end. b) Approximation of the displacements of the end of the beam.

To approximate the value of κ , let us assume that the end of a cantilever beam moves on the arc of a circle (see Fig. 1.11 b)). Then, by Pythagoras,

$$L^2 = (L - \xi)^2 + \eta^2 \quad \Rightarrow \quad \xi^2 - 2L\xi + \eta^2 = 0,$$

so ξ is given by

$$\xi = \frac{1}{2} \frac{\eta^2}{L} + \mathcal{O}(\eta^4). \quad (1.106)$$

The assumption provides the approximation of $\kappa = 1/(2L)$ where L denotes the length of the beam.

Let us consider the problem of Subsec. 1.3.1 assuming $M_z = 0$. Then the deformation function of the modelled beam in Fig. 1.11 a) is given by

$$v(x; Q_y) = \frac{Q_y}{\gamma IE} \left(\frac{\tan(\sqrt{\gamma}L)}{\sqrt{\gamma}} (1 - \cos(\sqrt{\gamma}x)) - \left(x - \frac{\sin(\sqrt{\gamma}x)}{\sqrt{\gamma}} \right) \right) \quad (1.107)$$

where its dependence on the lateral force Q_y is emphasized.

Then, the lateral deformation of the end of the beam η , is given by

$$\eta = v(L; Q_y) \quad (1.108)$$

from which the lateral force is obtained in the form

$$Q_y(\eta) = \frac{\gamma\sqrt{\gamma}IE}{\tan(\sqrt{\gamma}L) - \sqrt{\gamma}L}\eta.$$

The substitution of this into the solution Eq. (1.107) leads to the lateral deformation function $v(x; Q_y(\eta))$, and the arc-length of the deformed beam $\sigma(\eta)$ can also be calculated as a function of η :

$$\sigma(\eta) = \int_0^{L-\kappa\eta^2} \sqrt{1 + \left(\frac{\partial v(x; Q_y(\eta))}{\partial x}\right)^2} dx. \quad (1.109)$$

Its dependence on the end point lateral deformation η is complicated due to the presence of η in the upper limit of the definite integral, where κ is the unknown parameter we need to determine in Eq. (1.105). By means of the Leibniz's Theorem for differentiation of an integral [1]:

$$\frac{\partial}{\partial x} \int_{a(x)}^{b(x)} f(x, t) dt = \frac{\partial b(x)}{\partial x} f(x, b(x)) - \frac{\partial a(x)}{\partial x} f(x, a(x)) + \int_{a(x)}^{b(x)} \frac{\partial f(x, t)}{\partial x} dt,$$

the power series of σ can be expressed with respect to η in the form

$$\sigma(\eta) = \sigma(0) + \sigma'(0)\eta + \frac{1}{2!}\sigma''(0)\eta^2 + \dots,$$

where it is obvious that $\sigma(0) = L$ and $\sigma'(0) = 0$ because when $\eta = 0$, that is, the displacement of the end of the beam is zero, then gradient of the arc-length is zero, too. The second derivative of σ at zero can be considered as

$$\sigma''(0) = -2\kappa + \int_0^{L-\kappa\eta^2} \frac{\partial^2}{\partial \eta^2} \left(\sqrt{1 + \left(\frac{\partial y(x; Q_y(\eta))}{\partial x}\right)^2} \right) dx \Bigg|_{\eta=0}.$$

It assumes the form

$$\sigma(\eta) = L + (-2\kappa + \chi) \frac{\eta^2}{2!} + \dots, \quad (1.110)$$

where

$$\chi = \frac{\left(1 + \frac{1}{2} \cos(2\sqrt{\gamma}L)\right) \gamma L - \frac{3}{4} \sqrt{\gamma} \sin(2\sqrt{\gamma}L)}{(\sqrt{\gamma}L \cos(\sqrt{\gamma}L) - \sin(\sqrt{\gamma}L))^2}.$$

Because the beam is considered to be inextensible, the arc-length is L for all values of η , so from Eq. (1.110) we have that

$$\sigma(\eta) \equiv L \Leftrightarrow \kappa = \chi/2$$

is obtained from Eq. (1.110), and

$$\kappa = \frac{2(2 + \cos(2\sqrt{\gamma}L)) \gamma L - 3\sqrt{\gamma} \sin(2\sqrt{\gamma}L)}{8(\sqrt{\gamma}L \cos(\sqrt{\gamma}L) - \sin(\sqrt{\gamma}L))^2}. \quad (1.111)$$

The parameter γ depends on the compression P , and the parameter κ can be developed as a dimensionless power series of γ :

$$\kappa L = \frac{3}{5} + \frac{1}{175} (L^2\gamma) + \frac{1}{2625} (L^2\gamma)^2 + \dots, \quad (1.112)$$

where κ is normalized by the length of the beam L and $L^2\gamma$ represents the relative importance of compression to the proportional part of Euler buckling load. The coefficient κ in Eq. (1.105) agrees with the numerical evaluation of the formula in [5], which gives the value of 0.5988 that is a good approximation of $3/5$ at zero compression. There is 20% difference between this exact solution and the approximation of $1/2$ of the triangle in terms of the cantilever beam (see Eq. (1.106)). The non-zero compression obviously increases the magnitude of the longitudinal displacement of the rod as it is also expressed by formula (1.112) analytically.

When we have tension, the formula of Eq. (1.111) is modified

$$\kappa = \frac{\left(2 + \frac{1}{\cosh^2(\sqrt{\gamma}L)}\right) \gamma L - 3\sqrt{\gamma} \tanh(\sqrt{\gamma}L)}{4(\sqrt{\gamma}L - \tanh(\sqrt{\gamma}L))^2}. \quad (1.113)$$

The parameter κ can also be given by the power series of γ

$$\kappa L = \frac{3}{5} - \frac{1}{175} (L^2\gamma) + \frac{1}{2625} (L^2\gamma)^2 \mp \dots \quad (1.114)$$

The non-zero tension decreases the magnitude of the longitudinal displacement of the beam as we can see in Fig. 1.12. When $L^2\gamma$ tends to infinity, by using L'Hospital's rule, $\kappa L = 1/2$.

Note that Eqs. (1.112) and (1.114) are not uniformly valid when $Q_y = 0$ due to the assumption of the inextensible nature of the beam. The results were translated from [7].

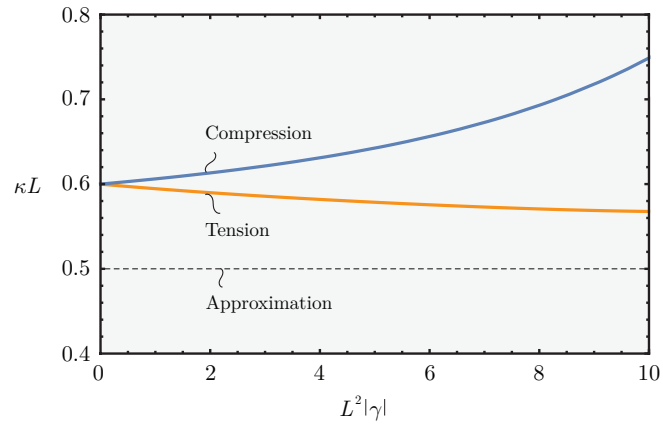


Figure 1.12: Dimensionless connection between the normalized κ and the relative importance of compression and tension.

Chapter 2

Dynamical Behaviour

The dynamical modelling follows the structure of Chap. 1, that is, it investigates how the introduced different types of loads affect the natural frequencies of the system. In the following, we are going to deal with one degree and two degrees of freedom systems. The basic model is a cantilever beam in tension or in compression, it has a block attached to its free end (see Fig. 2.1) on which torsion might also appear. Since semi-tangential torsion is the correct way to maintain the stability problems properly (see Subsec. 1.2.4), the natural frequency calculations are based on these models of torsion only. The difference between the one degree and the two degrees of freedom systems is related to the assumption whether the mass moment of inertia of the end block is negligible or not. The mass of the beam is also considered as a quantity to a body concentrated at the free end of the beam. The beam is either in compression (see Fig. 2.1 a)) or in tension (see Fig. 2.1 b)) depending on whether the structure stands upward or downward in the gravitational space, respectively. The horizontal arrangement refers to the neutral case.

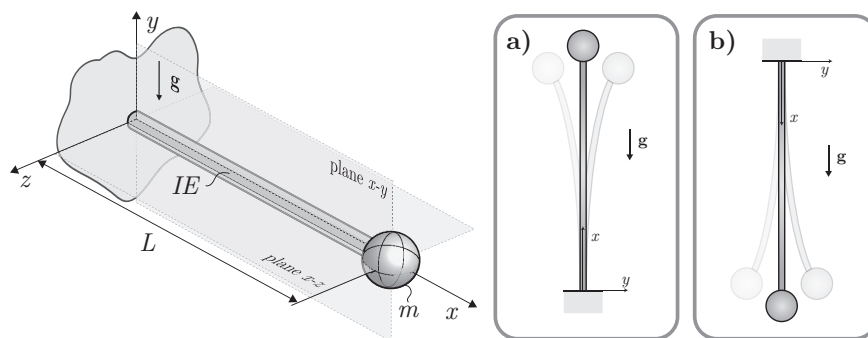


Figure 2.1: The arrangement of dynamical model. a) Case of compression. b) Case of tension.

The results of Chap. 1 are used to calculate stiffness characteristics, which are used to describe the bending vibrations. The natural frequency calculations take into account the variation of the stiffness of the beam, but some cases exploit the modification of the potential energy concerning the vertical position of the end block.

2.1 Approximating inertial effects

In this modelling section, the purpose is to investigate such a cantilever beam where its mass is taken into account in a block attached to its free end. The determination of this additional lumped mass can be calculated by means of the first natural angular frequency of a corresponding continuum rod (see Fig. 2.2).

The motion of the system is described by

$$\rho A \frac{\partial^2 v(x, t)}{\partial t^2} + IE \frac{\partial^4 v(x, t)}{\partial x^4} = 0, \quad (2.1)$$

where t denotes the time. By using the adequate boundary conditions, the natural angular frequencies of the system can be calculated as

$$\omega_{nk} = \frac{\beta_k^2}{L^2} \sqrt{\frac{IE}{\rho A}}. \quad (2.2)$$

For the first natural angular frequency, we have $\beta_1^2 = 3.533$. When the simple beam-mass structure is substituted by a one degree of freedom spring-mass system, then it yields

$$\frac{\beta_1^2}{L^2} \sqrt{\frac{IE}{\rho A}} = \sqrt{\frac{s}{m_0}}, \quad s = \frac{3IE}{L^3}. \quad (2.3)$$

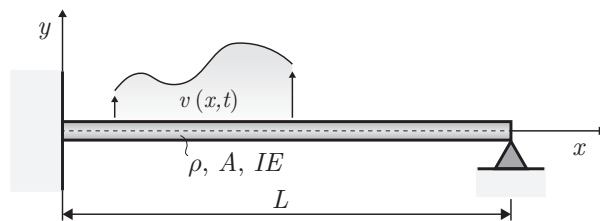


Figure 2.2: Model of the continuum beam.

Therefore, the value of the lumped mass is

$$m_1 = 0.2404m_0, \quad (2.4)$$

where the mass of the beam is denoted by m_0 . Basically, we consider a block attached to the free end of the beam, which mass m is purely equal with the concentrated mass m_1 of the beam but in some cases (see in Subsec. 2.2.2 and in Subsec. 2.2.3), an additional mass m_2 is assumed in order to manifest the effect of compression or tension. Thus in these cases $m = m_1 + m_2$. By using this end block, we will be able to deal with two degrees of freedom models if we take into account the mass moment of inertia.

2.2 Natural frequencies of the cantilever beam

The purpose is to consider the bending vibration of the cantilever beam and determine its natural frequencies. Their number depends on the assumed degree of freedom of the system. Our investigation examines only the linear vibration where the linearisation is determined around the equilibrium position of the structure.

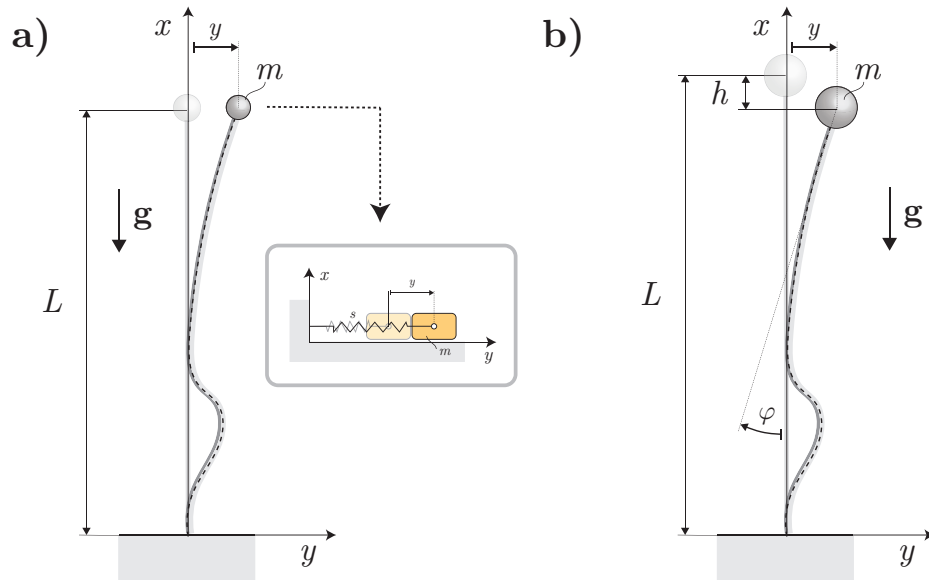


Figure 2.3: a) One degree of freedom dynamical model. b) Two degree of freedom dynamical model where the presence of h is also considered in some of the models.

The global system is depicted in Fig. 2.3 depending upon whether the mass moment of inertia of the end block is negligible or not. The generalised coordinates are defined by the horizontal displacement y and the angular rotation of the end of the beam denoted by φ .

Note that the results of the following subsections use the data summarized in Table 2.1.

Table 2.1: Data of the investigated system that are utilised at the calculation of the natural angular frequencies.

Notation	Designation	Value	Unit
ρ	Density of beam/end body	7900	kg/m ³
E	Young's modulus of beam	200	GPa
r	Radius of cross section	0.002	m
R	Radius of end body	0.030	m
L	Length of the beam	0.500	m
IE	Bending stiffness	2.513	Nm ²
m_2	Additional mass to the block	0.088	kg

2.2.1 Vibration of unloaded beam

The case of the unloaded system assumes that there are no tensile force, no compressive force and no torsional moment acting on the beam. In order to proceed, let us consider the deformation function of Eq. (1.65) where γ tends to zero. This yields

$$v(x) = \frac{x^2}{6IE}(3(M_z + Q_y L) - Q_y x), \quad (2.5)$$

which is used to determine a lumped stiffness parameter of the beam.

One Degree of Freedom System

By means of Eq. (2.5) and considering $M_z = 0$, an equivalent lateral stiffness

$$s = \frac{Q_y}{\delta_v} \quad (2.6)$$

can be calculated with respect to the free end of the beam. After substitutions, we obtain the well-known formula

$$s = \frac{3IE}{L^3}. \quad (2.7)$$

The equation of motion is given by

$$\ddot{y}(t) + \frac{s}{m}y(t) = 0, \quad (2.8)$$

where

$$\omega_n = \sqrt{\frac{s}{m}} \quad (2.9)$$

means the natural angular frequency of the system where the value of the end mass is $m = 0.012$ kg (it comes only from the mass of the beam, the additional mass m_2 is considered to be zero here) and its compressive effect is neglected because it stands in the neutral (horizontal) position, so $\omega_n = 71.098$ rad/s.

The determination of the natural angular frequencies of the system can also be approximated by taking into account the modification of the potential energy when the beam stands upward. Here, we can consider $h(t)$ that describes the vertical lifting of the mass m . The generalised coordinate is

$$q(t) = y(t). \quad (2.10)$$

To describe the motion of the system, we utilise the Lagrange's equation of motion of second kind

$$\frac{d}{dt} \frac{\partial T}{\partial \dot{y}} - \frac{\partial T}{\partial y} + \frac{\partial U}{\partial y} = 0. \quad (2.11)$$

The kinetic energy assumes the form

$$T = \frac{1}{2}mv_C^2(t). \quad (2.12)$$

where $v_C(t) = \text{col}(\dot{y}(t) \quad \dot{h}(t))$. The potential energy can be defined as

$$U = \frac{1}{2}sy^2(t) - mgh(y(t)), \quad (2.13)$$

where $h(y(t)) = \kappa y^2(t) + \dots$ and κ comes from Eq. (1.112). By using this step, we are able to transform our model to 1 DoF. Hence the linearised equation of motion can be written as

$$\ddot{y}(t) + \left(\frac{s - 2mg\kappa}{m} \right) y(t) = 0, \quad (2.14)$$

where

$$\omega_n = \sqrt{\frac{\frac{3IE}{L^3} - 2mg\kappa}{m}}. \quad (2.15)$$

The value of the end mass is still $m = 0.012$ kg, so $\omega_n = 70.932$ rad/s.

Two Degrees of Freedom System

The system can be seen in Fig. 2.3 b) where the vector of the generalised coordinates is given by

$$\mathbf{q}(t) = \begin{pmatrix} y(t) \\ \varphi(t) \end{pmatrix}. \quad (2.16)$$

In order to investigate the motion of the system, we need the kinetic energy

$$T = \frac{1}{2}mv_C^2(t) + \frac{1}{2}\theta_C\Omega^2(t), \quad (2.17)$$

where θ_C is the mass moment of inertia of the end body and Ω is the angular velocity that corresponds to $\dot{\varphi}$. The velocity of the centre of gravity of the end body is denoted by v_C that is approximated only by \dot{y} since \dot{h} is negligible here.

If the zero position of the potential function is defined at the centre of gravity of the end body in equilibrium, then the expression of the potential energy is

$$U = \frac{1}{2}\mathbf{q}^\top(t)\mathbf{S}_r\mathbf{q}(t) - mg\kappa y^2(t), \quad (2.18)$$

where \mathbf{S}_r is the stiffness matrix of the rod. It comes from the expression $\mathbf{S}_r = \mathbf{C}^{-1}$ where \mathbf{C} is the compliance matrix given by

$$\begin{aligned} \mathbf{C} &= \begin{pmatrix} \left. \frac{\partial U}{\partial Q_y} \right|_{Q_y=1, M_z=0} & \left. \frac{\partial U}{\partial Q_y} \right|_{Q_y=0, M_z=1} \\ \left. \frac{\partial U}{\partial M_z} \right|_{Q_y=1, M_z=0} & \left. \frac{\partial U}{\partial M_z} \right|_{Q_y=0, M_z=1} \end{pmatrix} \\ &\equiv \begin{pmatrix} \left. \frac{\partial \delta_v}{\partial Q_y} \right|_{M_z=0} & \left. \frac{\partial \delta'_v}{\partial Q_y} \right|_{M_z=0} \\ \left. \frac{\partial \delta_v}{\partial M_z} \right|_{Q_y=0} & \left. \frac{\partial \delta'_v}{\partial M_z} \right|_{Q_y=0} \end{pmatrix}. \end{aligned} \quad (2.19)$$

where U gives the strain energy of the system that is originated in bending only.

In terms of Eq. (2.17) and Eq. (2.18), the linear matrix coefficient differential equation assumes the form

$$\mathbf{M}\ddot{\mathbf{q}}(t) + \mathbf{S}\mathbf{q}(t) = \mathbf{0}, \quad (2.20)$$

where the mass matrix is denoted by \mathbf{M} and its form is

$$\mathbf{M} = \begin{pmatrix} m & 0 \\ 0 & \theta_C \end{pmatrix}. \quad (2.21)$$

The stiffness matrix is defined as

$$\mathbf{S} = \left. \frac{\partial^2 U}{\partial q_i \partial q_j} \right|_{\mathbf{q}=0}. \quad (2.22)$$

By means of Eq. (2.5), the stiffness matrix is expressed by

$$\mathbf{S} = \begin{pmatrix} \frac{12IE}{L^3} - 2mg\kappa & -\frac{6IE}{L^3} \\ -\frac{6IE}{L^3} & \frac{4IE}{L} \end{pmatrix}. \quad (2.23)$$

The natural frequencies of the system can be calculated by using the frequency equation, that is

$$\det(-\omega_n^2 \mathbf{M} + \mathbf{S}) = 0. \quad (2.24)$$

The expanded form of Eq. (2.24) is a bi-quadratic equation

$$\omega_n^4 - \left(\frac{4IE}{\theta_C L} + \frac{12\theta_C IE}{mL^3} - 2g\kappa \right) \omega_n^2 + \left(\frac{12(IE)^2}{m\theta_C L^4} - \frac{8IEg\kappa}{\theta_C L} \right) = 0, \quad (2.25)$$

where the expression of κ comes from Eq. (1.112). It gives two positive roots where $\omega_{n1} < \omega_{n2}$. By substituting the appropriate data from Table 2.1 and $m = 0.012$ kg (still $m_2 = 0$ kg) into Eq. (2.25) and considering the shape of the end body as a sphere, we obtain that $\omega_{n1} = 70.817$ rad/s and $\omega_{n2} = 2166.940$ rad/s.

When $\kappa = 0$, that is, we do not take into account the vertical lifting of the end mass (neutral case), we obtain that $\omega_{n1} = 70.983$ rad/s and $\omega_{n2} = 2166.940$ rad/s.

Comparison of results

The investigation of the one degree of freedom systems shows that the natural angular frequencies are lower when the beam is in upward vertical position and the value of κ is taken into account, correspondingly. It is caused by the vertical lifting $\kappa y^2(t)$ that decreases the stiffness of the system indirectly. The difference between the two calculations is not significant here, it is only 0.233%.

In case of the two degree of freedom systems, it can be shown that the comparison (either when $\kappa = 0$ or $\kappa \neq 0$) of their natural angular frequencies to the one degree of freedom system's gives 0.162% difference. So the mass moment of inertia has no significant effect on the natural angular frequencies

in both cases. It can also be seen that the lifting of the end mass has also effect on the natural angular frequencies but in case of the selected data, it is negligible at the second natural angular frequencies.

Table 2.2: Analytical results for the first and second natural angular frequencies of the systems by using the data of Table 2.1 and $m = 0.012$ kg.

Natural angular frequency	1 DoF System		2 DoF System	
	$\kappa = 0$	$\kappa \neq 0$	$\kappa = 0$	$\kappa \neq 0$
ω_{n1} (rad/s)	71.098	70.932	70.983	70.817
ω_{n2} (rad/s)	-	-	2166.940	2166.940

2.2.2 Beam in Compression

The dynamical model of the compressed cantilever beam can be seen in Fig. 2.23 b). The effect of compression or tension is manifested by the arrangement of the structure. There is an additional mass m_2 introduced in Sec. 2.1 which is to model the effect of compression. Thus the total mass m consists of the lumped mass m_1 of the rod and the mass m_2 . The importance of this mass m_2 will be seen in the laboratory tests (see Chap. 4).

Stiffness Variation

Henceforward, we are going to deal with the problem of stiffness variation and investigate how the natural frequencies of the system are affected by the applied loads. The simplest case is when the cantilever beam is in compression or tension. To proceed, we utilise Eq. (1.65) to define the stiffness variation.

One Degree of Freedom System

As it has been introduced in Subsec. 2.2.1, an equivalent lateral stiffness can be defined as the quotient of a lateral force that is perpendicular to the axis of the beam and the displacement of the end of the rod in the direction of the lateral force. The lateral displacement has already been specified in the MacLaurin-series of Eq. (1.67). The lateral force Q_y is emphasized here, thus it can be easily eliminated. So the analytical formula of the lateral stiffness variation yields

$$s = \frac{\gamma\sqrt{\gamma}IE}{\tan(\sqrt{\gamma}L) - \sqrt{\gamma}L}, \quad (2.26)$$

which can be approximated by the dimensionless power series

$$\frac{L^3}{IE}s = 3 - \frac{6}{5}(L^2\gamma) - \dots \quad (2.27)$$

Clearly, the compression decreases the lateral stiffness of the beam (see Fig. 2.4). Where the curve crosses the horizontal axis there is the first normalised Euler buckling load. Since only the stiffness of the system has changed, the equation of motion corresponds with Eq. (2.8) that yields

$$\omega_n = \sqrt{\frac{\gamma\sqrt{\gamma}IE}{m(\tan(\sqrt{\gamma}L) - \sqrt{\gamma}L)}} \quad (2.28)$$

where the compression constant γ obviously depends on the compressive force P . It is manifested by the end block, that is, $P = mg$. The mass of the end block is $m=0.1$ kg here and the natural angular frequency of the system is $\omega_n = 24.075$ rad/s.

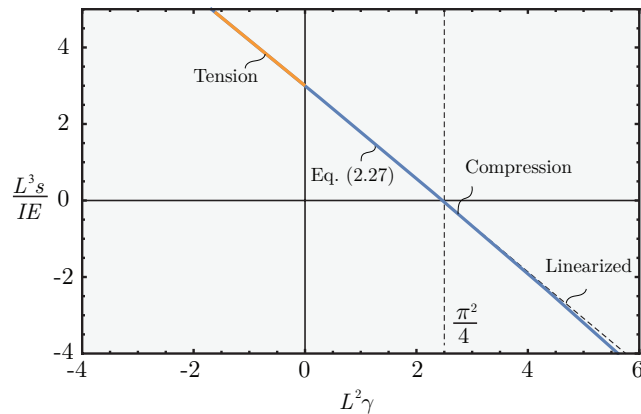


Figure 2.4: Dimensionless connection between relative importance of spring stiffness and the relative importance of compression/tension.

Two Degrees of Freedom System

Since the mass moment of inertia might have significant effect on the natural angular frequencies, we have to use a two degrees of freedom system and examine how the compression influences the compliance matrix.

First of all, let us consider the deformation function of a compressed cantilever beam described by Eq. (1.65) and use the definition of the compliance

matrix via Eq. (2.19). By performing the mathematical operations, we obtain

$$\mathbf{C} = \begin{pmatrix} \frac{\tan(\sqrt{\gamma}L)}{\gamma\sqrt{\gamma}IE} - \frac{L}{\gamma IE} & -\frac{1}{\gamma IE} \left(1 - \frac{1}{\cos(\sqrt{\gamma}L)}\right) \\ -\frac{1}{\gamma IE} \left(1 - \frac{1}{\cos(\sqrt{\gamma}L)}\right) & \frac{\tan(\sqrt{\gamma}L)}{\sqrt{\gamma}IE} \end{pmatrix}. \quad (2.29)$$

The stiffness matrix can be calculated by means of the compliance matrix. In order to have a better look related to the elements of the stiffness matrix, they are considered by their MacLaurin-series with respect to compressive force P

$$\mathbf{S} = \begin{pmatrix} \frac{12IE}{L^3} - \frac{6}{5L}P - \dots & -\frac{6IE}{L^2} + \frac{1}{10}P + \dots \\ -\frac{6IE}{L^2} + \frac{1}{10}P + \dots & \frac{4IE}{L} - \frac{2L}{15}P - \dots \end{pmatrix}. \quad (2.30)$$

As we can see, when compression P tends to zero, we can get back the well-known form of the stiffness matrix of an unloaded beam (no external forces).

To proceed, let us consider Eq. (2.20). The natural angular frequencies of the system can be calculated by using the frequency equation (see Eq. (2.24)) where the mass matrix correspond to Eq. (2.21).

If $m = 0.1$ kg, the natural angular frequencies of the system are $\omega_{n1} = 24.036$ rad/s and $\omega_{n2} = 747.327$ rad/s.

Potential Energy Variation

The theory of potential energy variation appeared in Subsec. 2.2.1, when we investigated the presence of the mass moment of inertia of the end block. The exact expression of the value of κ can be found in Eq. (1.111). By using the data of Table 2.1 and assuming that $m = 0.1$ kg, the reduced one degree of freedom system gives $\omega_n = 24.075$ rad/s.

If we take into account the mass moment of inertia of the end block, the bi-quadratic frequency equation (see Eq. (2.25)) does not change. When $m = 0.1$ kg, we obtain the natural angular frequencies $\omega_{n1} = 24.036$ rad/s and $\omega_{n2} = 748.543$ rad/s.

Comparison of results

First of all, we can conclude that the stiffness variation of the beam under compression corresponds to the potential energy variation of the system taking into account the vertical lifting of the end body. So if there is a lumped

mass at the free end of the vertical beam, the bending vibration frequency can be calculated either by means of this reduced lateral stiffness or by the variation of the potential energy of the lumped mass in the gravitational space due to the vertical deformation. In what follows, the nonlinear equivalence of the two approaches is proven.

Based on the numerical results of Table 2.3, it can be seen that the effect of the mass moment of inertia of the end block influences the natural angular frequencies of the system compared to the one degree of freedom systems. In case of the first natural angular frequency, this discrepancy is not significant (cca. 0.162%) but it obviously depends on the material and geometrical data of the system.

By comparing the second natural angular frequencies of the two degrees of freedom systems (summarised in Table 2.3), we can experience small discrepancy (cca. 0.162%) in between the results. The reason of the difference can be identified in the considered potential energy function Eq. (2.13) of the system. Since the vertical displacement h is assumed to depend only on the horizontal displacement x , we neglect the effect of a possible bending torque. It causes that when the compressive force P tends to its critical value $P_{cr} = \pi^2 IE / (2L)^2$, the determinant of \mathbf{S} (see Eq. (2.23)) - by using the exact value of κ (see Eq. (1.111)) - will not be zero, that is

$$\frac{3IE}{L^3} - 2P_{cr}\kappa = 0. \quad (2.31)$$

To approximate the critical value of compression, let us use the first approximation of κ (see the first term in Eq. (1.112)). Then the solution of Eq. (2.31) leads to $P_{cr} = 10IE / (2L)^2$ that means 1.3% difference compared to

Table 2.3: Analytical results (compression) for the first and second natural angular frequencies of the systems by using the data of Table 2.1 and $m = 0.1$ kg.

Natural angular frequency	1 DoF System			2 DoF System		
	Stiffness variation ($\kappa = 0$)	$\kappa \neq 0$	$P = 0$	Stiffness variation ($\kappa = 0$)	$\kappa \neq 0$	$P = 0$
ω_{n1} (rad/s)	24.075	24.075	24.560	24.036	24.036	24.520
ω_{n2} (rad/s)	-	-	-	747.327	748.543	748.543

the Euler critical buckling load $\pi^2 IE / (2L)^2$. The error decreases as the approximation of κ is improved. So the Euler critical value is obtained exactly if the additional tiny height variation h is calculated also as a function of the angle φ caused by a torque at the free end of the bar.

When $P = 0$, that is, there is no compression (neutral case), we have 1.974% (1 DoF system) difference between the neutral and compressed cases. By investigating the 2 DoF system, we experience 1.974% discrepancy in between the first natural angular frequencies (compressed-neutral) and there is cca. 0.162% discrepancy in between the second natural angular frequencies (compressed-neutral).

Proving with energy method

In the case of elastic bodies, the external forces are also going to perform work when the points of application of these forces are shifted by the effect of another applied force. The loads above are progressively increased from their zero values to their supreme values. Let us consider the point of application of \mathbf{Q}_y^i that moves with unit vector \mathbf{e}_i . If the relationship is linear between the load and the displacement then the performed work is

$$W_i = \frac{1}{2} \mathbf{Q}_y^i \mathbf{e}_i.$$

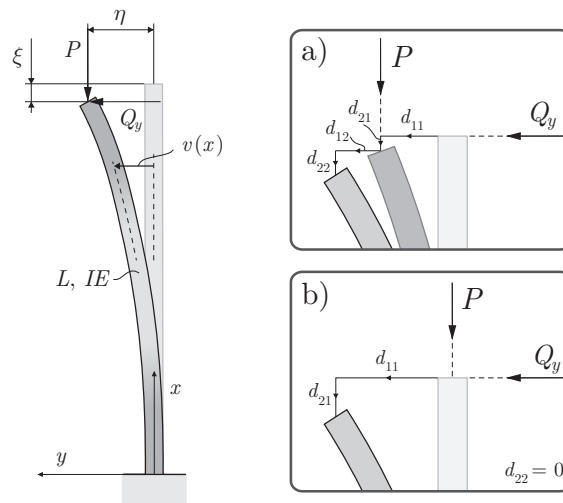


Figure 2.5: Displacement analysis. The displacements of d_{11} and d_{21} are affected by the lateral force Q_y . The d_{12} and d_{22} are due to compression P .

If d_i is a displacement component of \mathbf{e}_i in the force direction, it yields

$$W_i = \frac{1}{2} Q_y^i d_i.$$

According to the Betti's-theorem, if a balanced elastic body with arbitrary shape loaded sequentially by two different equilibrium force systems included forces and couples then they are signed by index 1 and index 2, respectively.

First of all, the elastic body is loaded by the force system of index 1 that is going to perform work W_{11} . After that we have to apply the force system of index 2, which also perform work W_{22} , however, the second force system gives rise to further strain, hence we need to take into account the work of the first force system, too, that provides another work signed by W_{12} . At the end of the loading period, the total work is

$$W = W_{11} + W_{22} + W_{12}, \quad (2.32)$$

where the proper work of the force systems is denoted by W_{11} and W_{22} as well as $W_{12} = W_{21}$ are extraneous works. Note that in this case the connection between the effects of forces and displacements are linear.

The aim is to prove that the strain energy of the described system defined by the stiffness of the beam corresponds with the work of external forces using the end displacements of the beam, that is, $U = W$. The strain energy can be written as

$$U = \frac{1}{2IE} \int_0^L M^2(x) dx, \quad (2.33)$$

where the function of the bending moment is defined by $M(x) = P\eta + Q_y\xi$. After the substitution of $M(x)$ and Eq. (1.107) into Eq. (2.33), we obtain

$$U = \frac{Q_y^2}{4\gamma\sqrt{\gamma}IE} \left(\frac{\sqrt{\gamma}L}{\cos^2(\sqrt{\gamma}L)} - \tan(\sqrt{\gamma}L) \right), \quad (2.34)$$

that can also be expressed by its power series with respect to compression P

$$U = \frac{Q_y^2 L^3}{IE} \left(\frac{1}{6} + \frac{2}{15} (L^2\gamma) + \frac{17}{210} (L^2\gamma)^2 + \dots \right). \quad (2.35)$$

The investigation of the work done by external forces is more complicated. In order to introduce some simplifications, let us consider Eq. (1.105) and Eq. (1.108) where the compression P is emphasized

$$\begin{aligned} \xi(P) &= \frac{Q_y^2(2\sqrt{\gamma}L(2 + \cos(2\sqrt{\gamma}L)) - 3\sin(2\sqrt{\gamma}L))}{8(IE)^2\gamma^2\sqrt{\gamma}\cos^2(\sqrt{\gamma}L)}, \\ \eta(P) &= \frac{Q_y(\tan(\sqrt{\gamma}L) - \sqrt{\gamma}L)}{IE\gamma\sqrt{\gamma}}. \end{aligned} \quad (2.36)$$

The forms of their power series yield

$$\xi(P) = \frac{Q_y^2 L^5}{(IE)^2} \left(\frac{1}{15} + \frac{17}{315} (L^2 \gamma) + \frac{31}{945} (L^2 \gamma)^2 + \dots \right) \quad (2.37)$$

and

$$\eta(P) = \frac{Q_y L^3}{IE} \left(\frac{1}{3} + \frac{2}{15} (L^2 \gamma) + \frac{17}{315} (L^2 \gamma)^2 + \dots \right), \quad (2.38)$$

respectively.

The first case can be seen in Fig. 2.5 a), we assume the lateral force Q_y is the first force as well as the compression P is the second one. Note that the extraneous works are not equal, hence the supposition of the Betti's-theorem that all forces are linear in the displacements does not hold. Henceforth Fig. 2.6 a) and Eq. (2.32) will be referred to frequently.

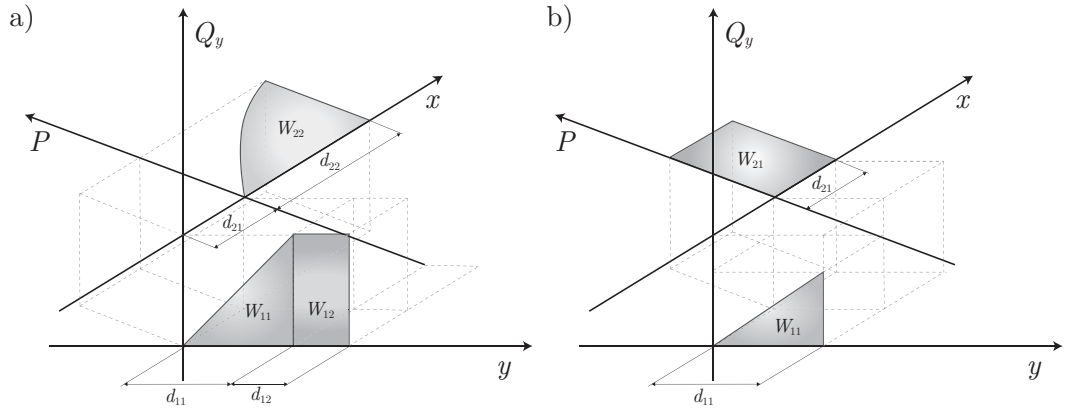


Figure 2.6: Works of external forces.

The lateral force is applied first that gives rise to two displacements in different directions but only one of them provides work because we do not even have compression. Since the relationship between Q_y and d_{11} is linear

$$W_{11} = \frac{1}{2} Q_y d_{11} = \frac{1}{2} Q_y \eta(0) = \frac{Q_y^2 L^3}{6IE}, \quad (2.39)$$

that means the area of a triangle in Fig. 2.6 a). The situation is more complicated in the case of W_{22} because the connection here is nonlinear,

thus

$$\begin{aligned}
 W_{22} &= \int_0^L P dx \\
 &= P(\xi(P) - \xi(0)) - \int_0^P \xi(P) - \xi(0) dP \\
 &= \frac{Q_y^2 \left(\sqrt{\gamma}L \left(12 + 2\gamma L^2 + \frac{3}{\cos^2(\sqrt{\gamma}L)} \right) - 15 \tan(\sqrt{\gamma}L) \right)}{12IE\gamma\sqrt{\gamma}},
 \end{aligned} \tag{2.40}$$

that is given by its power series

$$W_{22} = \frac{Q_y^2 L^3}{IE} \left(\frac{17}{630} (L^2\gamma)^2 + \frac{62}{2835} (L^2\gamma)^3 + \dots \right). \tag{2.41}$$

The reason of the way of the calculation is that ξ depends on compression but we need to calculate the area of W_{22} (see Fig. 2.6 a)). Finally, we examine W_{12} . The displacement is caused by compression P in the direction of the lateral force Q_y that means a rectangular area in $Q_y - y$ plane hence the connection is also linear

$$\begin{aligned}
 W_{12} &= Q_y(\eta(P) - \eta(0)) \\
 &= -\frac{Q_y^2(3\sqrt{\gamma}L + \gamma\sqrt{\gamma}L^3 - 3\tan(\sqrt{\gamma}L))}{3IE\gamma\sqrt{\gamma}}
 \end{aligned} \tag{2.42}$$

expressed by its power series

$$W_{12} = \frac{Q_y^2 L^3}{IE} \left(\frac{2}{15} (L^2\gamma) + \frac{17}{315} (L^2\gamma)^2 + \dots \right). \tag{2.43}$$

The summation of Eqs. (2.39), (2.40) and (2.42) provides

$$W = \frac{Q_y^2}{4\gamma\sqrt{\gamma}IE} \left(\frac{\sqrt{\gamma}L}{\cos^2(\sqrt{\gamma}L)} - \tan(\sqrt{\gamma}L) \right) \tag{2.44}$$

given by its power series

$$W = \frac{Q_y^2 L^3}{IE} \left(\frac{1}{6} + \frac{2}{15} (L^2\gamma) + \frac{17}{210} (L^2\gamma)^2 + \dots \right), \tag{2.45}$$

that exactly corresponds with the strain energy (see Eq. (2.34) and (2.35)).

The second case can be seen in Fig. 2.5 b) where compression P is assumed to be the first force. As we consider the stiffness of the beam is infinitely large in the beam direction, thus compression does not cause displacement ($d_{22} = 0$) that implies $W_{22} = 0$. When the lateral force Q_y appears, it causes two displacements d_{11} and d_{21} . The work W_{11} is actually the area of a triangle because Q_y was increased uniformly up to its supreme value

$$\begin{aligned} W_{11} &= \frac{1}{2} Q_y \eta(P) \\ &= \frac{Q_y^2 (\tan(\sqrt{\gamma}L) - \sqrt{\gamma}L)}{2IE\gamma\sqrt{\gamma}} \end{aligned} \quad (2.46)$$

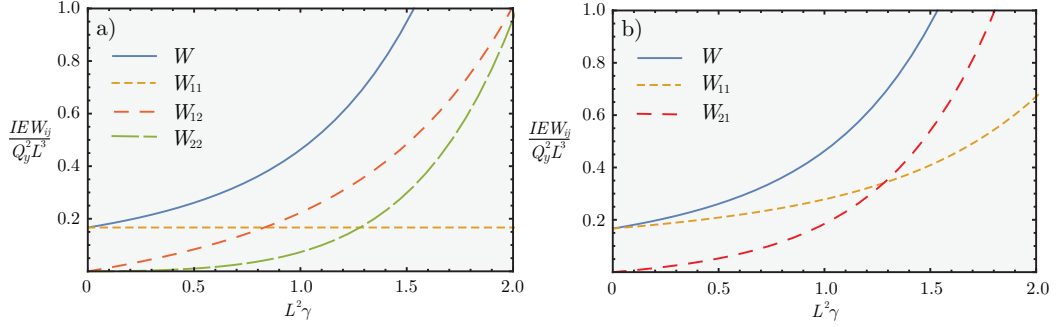


Figure 2.7: Dimensionless connection between the normalized works and the relative importance of compression. (a) Case 1. (b) Case 2.

expressed by its power series

$$W_{11} = \frac{Q_y^2 L^3}{IE} \left(\frac{1}{6} + \frac{1}{15} (L^2\gamma) + \frac{17}{630} (L^2\gamma)^2 + \dots \right). \quad (2.47)$$

The work W_{21} can be defined as a rectangular area (see Fig. 2.6 b)) because the value of compression was constant during the application of F

$$\begin{aligned} W_{21} &= P\xi(P) \\ &= \frac{Q_y^2 (2\sqrt{\gamma}L(2 + \cos(2\sqrt{\gamma}L)) - 3\sin(2\sqrt{\gamma}L))}{8IE\gamma\sqrt{\gamma}\cos^2(\sqrt{\gamma}L)}, \end{aligned} \quad (2.48)$$

given by its power series

$$W_{21} = \frac{Q_y^2 L^3}{IE} \left(\frac{1}{15} (L^2\gamma) + \frac{17}{315} (L^2\gamma)^2 + \dots \right). \quad (2.49)$$

The summation of Eqs. (2.46) and (2.48) provides the same result such as (2.44).

So the effect of the displacement in the rod direction results in the same potential energy variation as the equivalent stiffness modification by loads. It can be seen in Fig. 2.7, too.

2.2.3 Beam in Tension

The mechanical model of the tensed cantilever beam is nearly the same that can be seen in Fig. 2.3 b). The effect of the tensile force can be modelled by the arrangement of the structure when it stands downward and the effect of the end mass behaves in tension.

Stiffness Variation

As it was already mentioned in Subsec. 2.2.2, tension means one of the simplest case related to the stiffness variation of the system. To proceed, we will use Eq. (1.71) to specify the equivalent stiffness of the beam.

One Degree of Freedom System

Similarly to Subsec. 2.2.2, an equivalent lateral stiffness can be introduced by means of Eq. (2.6) that implies

$$s = \frac{\gamma\sqrt{\gamma}IE}{\sqrt{\gamma}L - \tanh(\sqrt{\gamma}L)}, \quad (2.50)$$

which can be given by the dimensionless power series

$$\frac{L^3}{IE}s = 3 + \frac{6}{5}(L^2\gamma) \pm \dots \quad (2.51)$$

To investigate the stiffness function s , let us have a look at Fig. 2.4. Since tension is only a change of sign of P compared to compression, if we increase the magnitude of tensile force, the lateral stiffness also increases and will not imply a critical value that could cause the failure of the structure. According to Eq. (2.9), the natural angular frequency of the system can be calculated

$$\omega_n = \sqrt{\frac{\gamma\sqrt{\gamma}IE}{m(\sqrt{\gamma}L - \tanh(\sqrt{\gamma}L))}}. \quad (2.52)$$

When the mass of the end block is $m = 0.1$ kg, $\omega_n = 25.034$ rad/s.

Two Degrees of Freedom System

The difference between the compression and tension is indicated only in the deformation function of the beam, thus the compliance matrix of the beam also changes. By using the definition (see Eq. (2.19)) and performing the operations, we obtain

$$\mathbf{C} = \begin{pmatrix} \frac{L}{\gamma IE} - \frac{\tanh(\sqrt{\gamma}L)}{\gamma\sqrt{\gamma}IE} & \frac{1}{\gamma IE} \left(1 - \frac{1}{\cos(\sqrt{\gamma}L)}\right) \\ \frac{1}{\gamma IE} \left(1 - \frac{1}{\cos(\sqrt{\gamma}L)}\right) & \frac{\tanh(\sqrt{\gamma}L)}{\sqrt{\gamma}IE} \end{pmatrix}. \quad (2.53)$$

The stiffness matrix also needs to be examined. It is derived from the compliance matrix. In order to have a better look associated with the elements of the stiffness matrix they are considered by their MacLaurin-series with respect to tension P

$$\mathbf{S} = \begin{pmatrix} \frac{12IE}{L^3} + \frac{6}{5L}P \mp \dots & -\frac{6IE}{L^2} - \frac{1}{10}P \pm \dots \\ -\frac{6IE}{L^2} - \frac{1}{10}P \pm \dots & \frac{4IE}{L} + \frac{2L}{15}P \mp \dots \end{pmatrix}. \quad (2.54)$$

As we can see, when tension tends to zero, we can get back the well-known form of the stiffness matrix of an unloaded beam.

To proceed, let us consider Eq. (2.20). The natural angular frequencies of the system can be calculated by using the frequency equation (see Eq. (2.24)) where the mass matrix correspond with Eq. (2.21).

If $m = 0.1$ kg, the natural angular frequencies of the system are $\omega_{n1} = 24.994$ rad/s and $\omega_{n2} = 749.754$ rad/s.

Potential Energy Variation

The case of potential energy variation can be similarly maintained such as in Subsec. 2.2.2. Since tension can be defined as a negative compression, to proceed, we will consider Eq. (1.113) to determine the modification of the potential energy. By using the data of Table 2.1 and assuming that $m = 0.1$ kg, the reduced one degree of freedom system gives $\omega_n = 25.034$ rad/s.

In this case, when we take into account the mass moment of inertia of the end body, the bi-quadratic frequency equation (see Eq. (2.25)) changes because the potential energy of the system (see Eq. (2.18)) now increases by the quantity mgh . By using $m = 0.1$ kg, we obtain the natural angular frequencies $\omega_{n1} = 24.994$ rad/s and $\omega_{n2} = 748.543$ rad/s.

Comparison of results

Based on the numerical results of Table 2.4, it can be seen that the effect of the mass moment of inertia of the end body influences the natural angular frequencies of the system compared to the one degree of freedom systems. This tiny discrepancy is cca. 0.161% in case of the first natural angular frequency.

By comparing the second natural angular frequencies of the two degrees of freedom systems (summarised in Table 2.4), we can experience the same discrepancy (cca. 0.161%) in between the results.

When $P = 0$, that is, there is no tension (neutral case), we have 1.896% (1 DoF system) difference between the neutral case and case of tension. By investigating the 2 DoF system, we experience 1.896% discrepancy in between the first natural angular frequencies (tension-neutral) and there is cca. 0.161% discrepancy in between the second natural angular frequencies (tension-neutral).

Table 2.4: Analytical results (tension) for the first and second natural angular frequencies of the systems by using the data of Table 2.1 and $m = 0.1$ kg.

Natural angular frequency	1 DoF System			2 DoF System		
	Stiffness variation ($\kappa = 0$)	$\kappa \neq 0$	$P = 0$	Stiffness variation ($\kappa = 0$)	$\kappa \neq 0$	$P = 0$
ω_{n1} (rad/s)	25.034	25.034	24.560	24.994	24.994	24.520
ω_{n2} (rad/s)	-	-	-	749.754	748.543	748.543

Note that the equivalence of the strain energy of the system and the works of external forces can also be proven here by using Betti's theorem.

2.2.4 Twisted Beam

In the following, we are going to take into account the effect of torsion. The dynamical models do not change compared to the previously investigated cases and they can be seen in Fig. 2.23. The lumped mass m_1 of the beam also appears but its compressive effect is neglected (and $m_2 = 0$ kg here) because the beam is in the neutral (horizontal) position. When we investigate our models in the presence of torsion, we consider only the theory of stiffness variation of the beam and its effect on the natural frequencies.

One Degree of Freedom System

As we previously did, we also utilise the theory of the equivalent spring stiffness here that is defined by Eq. (2.6). Since we have already investigated the deformation of the beam subjected to torsion, we only need to consider Eq. (1.90) to specify the spring stiffness s . Eq. (1.90) describes the displacement of the end of the beam in the direction of the lateral force vector. Let us assume that $\Gamma = 0$ and $\Lambda = Q_y/(IE)$, that is, $Q_z = 0$. It is needed to mention that $\delta_v = \text{Re}(d_L)$. Therefore, we obtain

$$s = \frac{2IE\alpha^3}{(4 + \alpha^2L^2) \tan\left(\frac{\alpha L}{2}\right) - 2\alpha L}, \quad (2.55)$$

that can be transformed to a dimensionless expression

$$\frac{L^3}{IE}s = \frac{2(\alpha L)^3}{(4 + (\alpha L)^2) \tan\left(\frac{\alpha L}{2}\right) - 2\alpha L}. \quad (2.56)$$

To check our results, let us have a look at Fig. 2.8 that actually shows the critical loads of the system and indicates how the stiffness modifies with respect to non-dimensional semi-tangential torsion. We can see that curve 1 tends to the line $L^3s/(IE) = 3$ and curve 2, 3 are asymptotic to the values of $\alpha L = 6.811$ and $\alpha L = 12.868$, respectively. The roots along the αL axis are the normalized critical loads of semi-tangential torque $(2n + 1)\pi$ where $n = 0, 1, \dots$ (see Subsec. 1.2.4).

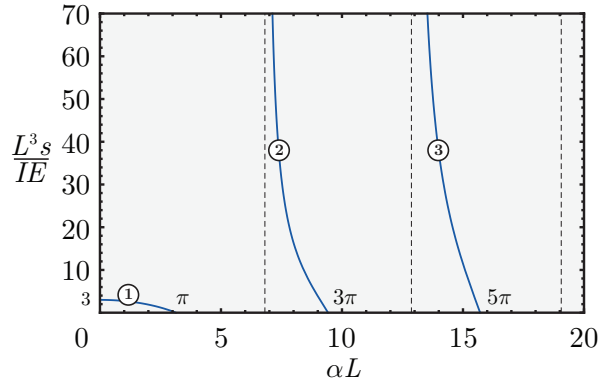


Figure 2.8: Dimensionless relation between the the relative importance of lateral stiffness and the relative importance of semi-tangential torsion.

To provide a better look in terms of the stiffness variation, the dimensionless power series of Eq. (2.56) is given by

$$\frac{L^3}{IE} s = 3 - \frac{21}{80}(\alpha L)^2 - \frac{151}{44800}(\alpha L)^4 + \dots \quad (2.57)$$

Clearly, the semi-tangential torsion decreases the lateral stiffness of the beam. Since only the stiffness of the system has changed, the equation of motion corresponds to Eq. (2.8) that yields

$$\omega_n = \sqrt{\frac{2IE\alpha^3}{m((4 + \alpha^2 L^2) \tan\left(\frac{\alpha L}{2}\right) - 2\alpha L)}}, \quad (2.58)$$

where the twist constant α obviously depends on the twisting torque M_t . By using the data of Table 2.1, the natural angular frequency of the system is depicted in Fig. 2.9 a).

Two Degrees of Freedom System

The mass moment of inertia may affect the natural frequencies, hence why we consider a two degrees of freedom system and specify the compliance matrix of the beam. To proceed, we need to take into account the deformation function of a beam subjected to semi-tangential torsion (see Eq. (1.89)). According to this and assuming that $Q_z = 0$ and $M_y = 0$, we obtain

$$\mathbf{C} = \begin{pmatrix} \frac{(4 + \alpha^2 L^2) \tan\left(\frac{\alpha L}{2}\right) - 2\alpha L}{2IE\alpha^3} & \frac{L \tan\left(\frac{\alpha L}{2}\right)}{IE\alpha} \\ \frac{L \tan\left(\frac{\alpha L}{2}\right)}{IE\alpha} & \frac{2 \tan\left(\frac{\alpha L}{2}\right)}{IE\alpha} \end{pmatrix}. \quad (2.59)$$

The stiffness matrix also needs to be examined that comes from the compliance matrix. The stiffness matrix is given by its MacLaurin-series with respect to torsion M_t

$$\mathbf{S} = \begin{pmatrix} \frac{12IE}{L^3} - \frac{6}{5IEL}M_t^2 - \dots & -\frac{6IE}{L^2} + \frac{3}{5IE}M_t^2 + \dots \\ -\frac{6IE}{L^2} + \frac{3}{5IE}M_t^2 + \dots & \frac{4IE}{L} - \frac{23L}{60IE}M_t^2 - \dots \end{pmatrix}. \quad (2.60)$$

By using the frequency equation, the natural angular frequencies of the system can be seen in Fig. 2.9 b). Their initial values - when $M_t = 0$ - correspond with the results of Table 2.2. Where the curves would cross the M_t axis, the first critical value of M_t can be found.

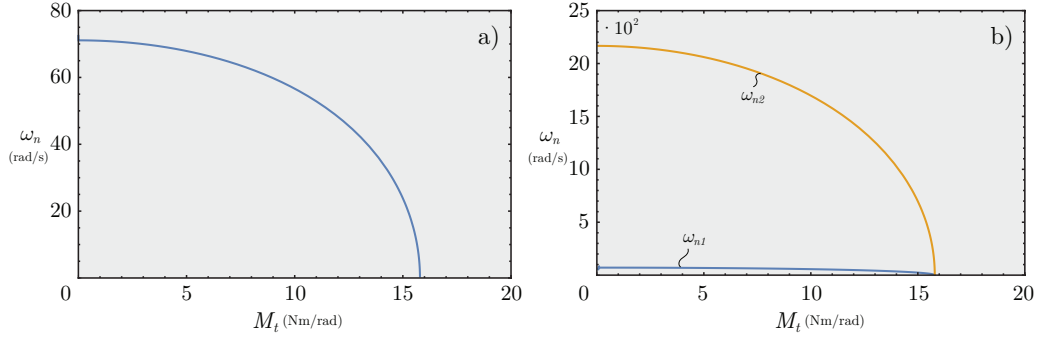


Figure 2.9: Natural angular frequency in case of a twisted beam ($m = m_1$ here). a) One degree of freedom system. b) Two degree of freedom system.

2.2.5 Twisted and Compressed Beam

The examination now considers a twisted and compressed shaft and provides results how the presence of the combined loads influences the natural frequencies of the system. The effect of compression does not come from the mass of end block here (neutral position), we just apply the compressive force P at the end of the shaft without using the additional mass m_2 . Since every single case has already been investigated separately, we might compare these results to the simpler ones.

One Degree of Freedom System

According to the expression of Eq. (2.6)), we are able to specify the equivalent lateral stiffness of the beam under torsion and compression by using Eq. (1.99) at $x = L$. Assuming that $Q_z = 0$ and $M_y = 0$, we obtain

$$s = - \frac{\nu\gamma^2 IE}{\nu\gamma L + \nu\alpha \frac{\sin(\mu L)}{\cos(\nu L)} - (2\nu^2 - \gamma) \tan(\nu L)}, \quad (2.61)$$

where

$$\mu = \alpha/2, \quad \nu = \sqrt{\alpha^2 + 4\gamma}/2.$$

When α , that is, the torsional constant tends to zero, then we arrive back to Eq. (2.26). In that case, when γ tends to zero, we need to apply L'Hospital's

rule to get Eq. (2.55). Similarly as we have previously made, the natural angular frequency of the system assumes the form

$$\omega_n = \sqrt{\frac{\nu\gamma^2 IE}{m(\nu\gamma L + \nu\alpha \frac{\sin(\mu L)}{\cos(\nu L)} - (2\nu^2 - \gamma) \tan(\nu L))}}. \quad (2.62)$$

By using the data of Table 2.1, the natural angular frequency of the system can be seen in Fig. 2.10. Since the resolution of the numerical calculation (applying only simple *for* loops for the values of compression P and torsion M_t) was not appropriate, we obtained a zig-zag curve in the vicinity of the parabolic line at the zero natural angular frequency. This also means the stability boundary of the system (see Fig. 2.10 a)) and corresponds to Fig. 1.4. Due to the simplicity of the one degree of freedom system, an analytical solution also could be found, which is depicted in Fig. 2.10 b). It can be seen that both compression P and torsion M_t decreases the natural angular frequency of the system up to their critical values.

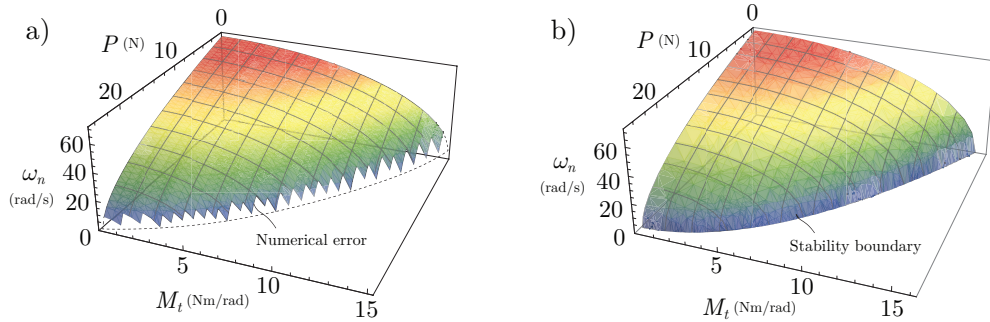


Figure 2.10: Natural angular frequency of the system under torsion M_t and compression P ($m = m_1$ here). a) Result of the numerical approximation. b) Analytical result.

Two Degrees of Freedom System

Let us assume a two degrees of freedom system and numerically specify its compliance matrix because of its complexity. By using the numerical compliance matrix, the stiffness matrix can also be given. To provide the natural angular frequencies of the dynamical system, we need to consider the frequency equation (see Eq. (2.24)). Therefore, the maps of the natural angular frequencies can be seen in Fig. 2.11. The stability boundary can also be discovered in both maps. We note that the stability boundary could be

approximated in a more accurate way by increasing the resolution of the numerical calculation (using two *for* loops for the values of compression P and torsion M_t).

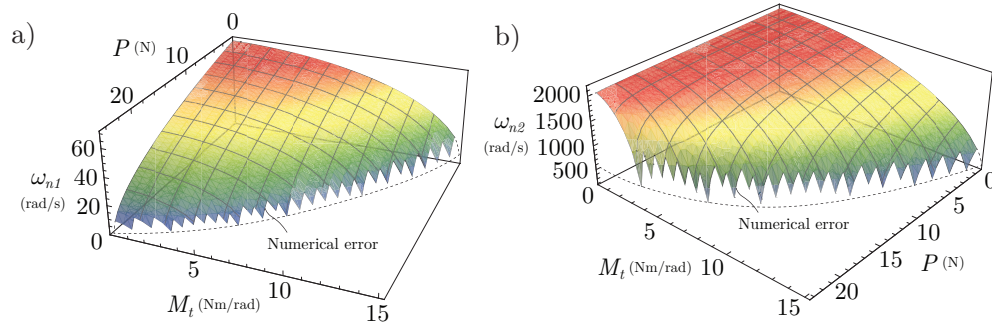


Figure 2.11: Natural angular frequencies of the two degree of freedom system under torsion M_t and compression P ($m = m_1$ here). a) Result of the numerical approximation of the first natural angular frequency. b) Result of the numerical approximation of the second natural angular frequency.

2.2.6 Twisted and Tensed Beam

Since the investigation of neither the purely twisted nor the twisted and compressed beam provided significant difference in between the natural frequencies, - so the mass moment of inertia of the end body had no real effect - henceforth, we take into account only the one degree of freedom system in case of a twisted and tensed beam.

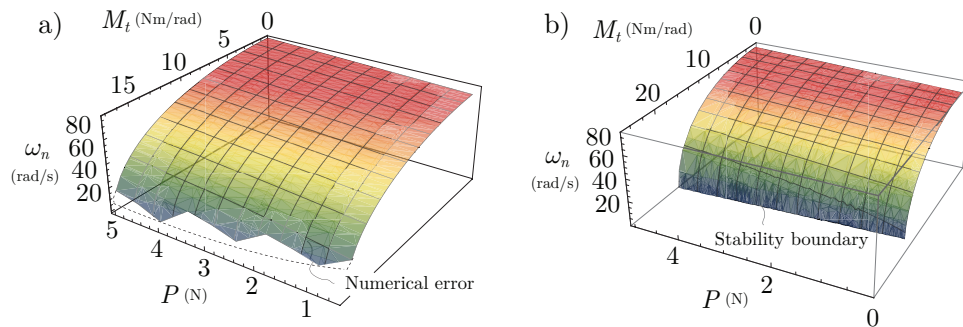


Figure 2.12: Natural angular frequencies of the twisted and tensed beam ($m = m_1$ here). a) Result of the numerical approximation. b) Analytical result.

By using Eq. (1.104) at $x = L$ and assuming that $Q_z = 0$ and $M_y = 0$, the lateral stiffness can be determined. By comparing this to Eq. (2.61), the only difference that reveals, is sign of γ .

The results are depicted in Fig. 2.12, where the stability boundaries also can be seen and it correlates with the results of Fig. 1.4 when $p < 0$. The presence of tension slightly increases the natural angular frequency of the system that implies a widening stable zone.

To summarise our results, let us have a look at Fig. 2.13 that introduces the entire frequency map in terms of compression/tension P and torsion M_t . The diagram looks like a half cup showing that the reduction of compression or the growth of tension increases the area of the stable zone. When M_t and P are zero, we arrive back to the results of Table 2.2. When $M_t \neq 0$ but $P = 0$, we are along the axis M_t and the result corresponds to Fig. 2.9 a). On the other hand, when $M_t = 0$ but $P \neq 0$, we are along the axis P and also get a parabolic curve.

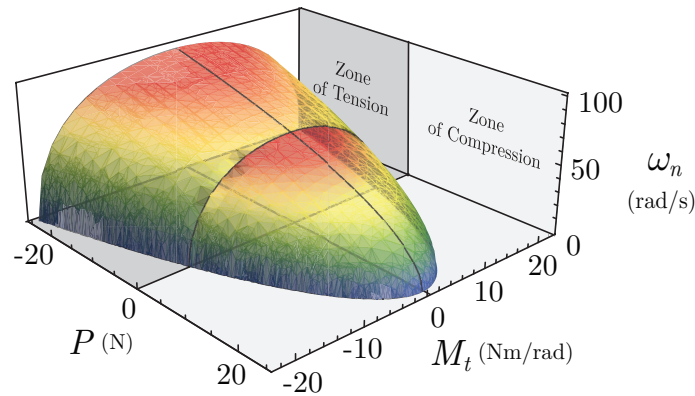


Figure 2.13: Variation of natural angular frequency of a twisted and compressed/tensed beam.

Chapter 3

Investigation of a light rotating beam

3.1 Modelling

Consider a long boring or a milling tool (see Fig. 3.1 a)) modelled by a straight vertical cantilever beam. The beam rotates about its vertical axis as well as being subjected to torsion M_t and compression $m\mathbf{g}$. Due to the presence of torsion, we are not able to analyse the system in two-dimensions [29]. The compression can be modelled by a lumped mass m attached to the free end of the beam (see Fig. 3.2 a)) that is much larger than the mass of the beam. Thus, the mass of the beam might be neglected. The beam is considered to be prismatic, homogeneous, linearly elastic and inextensible. It is either in compression or in tension depending on whether it stands upward or downward, respectively. The described system might become unstable depending upon the speed of rotation, the compression, torsion or a combination of all three [29].

The arrangement of the model and the corresponding notation can be seen in Fig. 3.2 a) where the gravitational acceleration is denoted by \mathbf{g} , the angular velocity is ω , the centrifugal force is $m\omega^2\mathbf{d}_1$, the compression is $m\mathbf{g}$ and the torsional moment vector is \mathbf{M}_t . Note that the twisting moment is assumed to be semi-tangential [30, 4] depicted in Fig. 3.1 b), that is, the forces F acting on the beam generate an axial torque \mathbf{M}_t that is able to tilt about both the y and z axes. By taking into account only small displacement $\mathbf{d} = \text{col}(v \ w)$ and angles ψ, θ during buckling, the linearised form of the torque is $\mathbf{M}_t = M_t \text{col}(1 \ \delta'_v/2 \ \delta'_w/2)$ (see also in Subsec. 1.1.2) where $M_t = 4Fa$, and the bending components of \mathbf{M}_t come from its resolution with respect to the principal system (ξ, η, ζ) and by using the definition of

the semi-tangential torque in the sense of Subsec. 1.1.2 (see Fig. 3.1 b) and c)). In case of the principal system, we consider ξ to be tangential to the deflected beam, while η is parallel to the $(x - y)$ plane and ζ is parallel to the $(x - z)$ plane. The notations δ'_v and δ'_w define the corresponding angular rotations of the end of the beam (see Fig. 3.2 a)).

The mathematical model is obtained using the Euler-Bernoulli connection between curvature and bending moment [3]

$$\frac{\partial\theta(\tilde{s})}{\partial\tilde{s}} = -\frac{M_z(\tilde{s})}{IE}, \quad \frac{\partial\psi(\tilde{s})}{\partial\tilde{s}} = -\frac{M_y(\tilde{s})}{IE}, \quad (3.1)$$

where the slope angles in the direction y and z are defined by θ and ψ (see Fig. 3.2 b)), respectively, and \tilde{s} is the arc length coordinate. The bending moment functions $M_{y,z}(\tilde{s})$ are expressed about y axis and z axis as follows:

$$M_y(\tilde{s}) = -M_t\theta(\tilde{s}) + mg\tilde{s}\psi(\tilde{s}) - mg\delta_w + m\omega^2\delta_w(\tilde{s} - L) + \frac{1}{2}M_t\delta'_v, \quad (3.2)$$

$$M_z(\tilde{s}) = M_t\psi(\tilde{s}) + mg\tilde{s}\theta(\tilde{s}) - mg\delta_v + m\omega^2\delta_v(\tilde{s} - L) - \frac{1}{2}M_t\delta'_w,$$

where δ_v and δ_w are displacements at the end of the beam. Since the variation of the torsional moment (the projection of \mathbf{M}_t to ξ) is of second order, the torsional stiffness of the beam is irrelevant from the viewpoint of buckling [3].

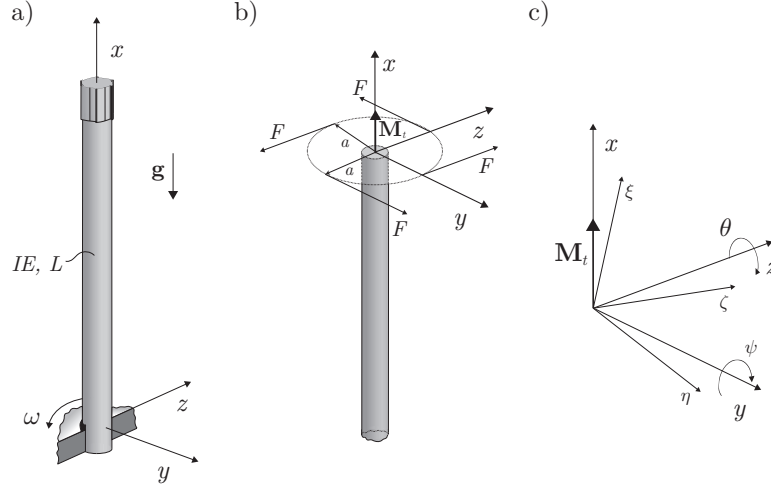


Figure 3.1: a) Model of the rotating tool. b) Concept of the semi-tangential moment in the sense of Ziegler [30]. c) Formulation of torsion.

The dimensionless length coordinate $s = \tilde{s}/L$ is normalised by the length L of the beam. By taking into account Eqs. (3.1) and (3.2), and neglecting

the nonlinear terms of the bending functions above, the bending moment balance gives the dimensionless differential equation system [27, 14, 3] for small θ and ψ in the form

$$\begin{aligned} \frac{\partial^2 \theta(s)}{\partial s^2} + \alpha' \frac{\partial \psi(s)}{\partial s} + \gamma' \theta(s) + \chi \delta_v &= 0, \\ \frac{\partial^2 \psi(s)}{\partial s^2} - \alpha' \frac{\partial \theta(s)}{\partial s} + \gamma' \psi(s) + \chi \delta_w &= 0, \end{aligned} \quad (3.3)$$

where the parameter $\alpha' = M_t L / IE$ specifies the relative importance of torsion to bending stiffness, $\gamma' = mgL^2 / IE$ is the relative importance of gravity to bending stiffness and $\chi = m\omega^2 L^3 / IE$ is the relative importance of rotation to bending stiffness.

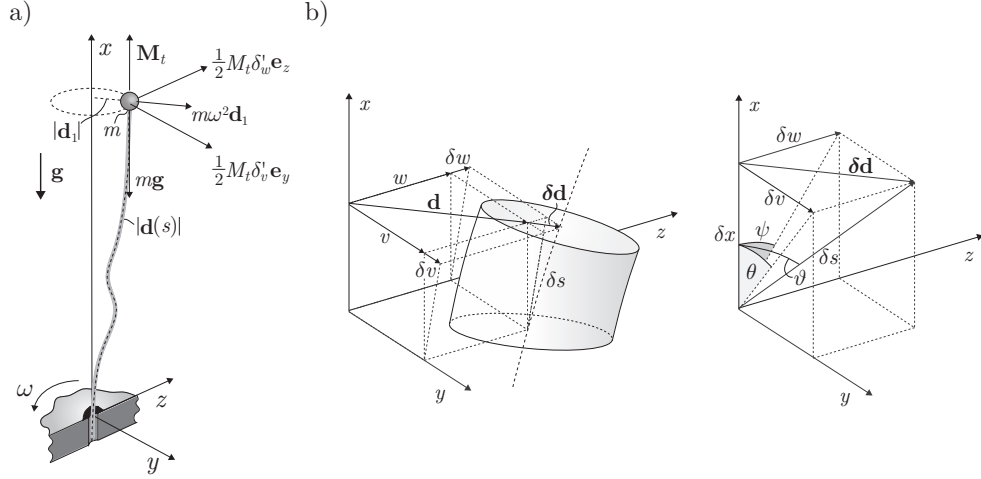


Figure 3.2: a) Rotating beam subjected to torsion and compression. b) Infinitesimal piece of the beam.

Let us introduce a complex function $r(s) = \theta(s) + i\psi(s)$. Hence from Eq. (3.2) we have

$$\frac{\partial^2 r(s)}{\partial s^2} - i\alpha' \frac{\partial r(s)}{\partial s} + \gamma' r(s) + \chi d_1 = 0, \quad (3.4)$$

where $d_1 = \delta_v + i\delta_w$ and $\mathbf{d}_1 = \text{col}(\delta_v \ \delta_w)$. The boundary conditions are

$$\begin{aligned} \theta(0) &= 0, & \left. \frac{\partial \theta(s)}{\partial s} \right|_{s=1} &= -\frac{1}{2} \alpha' \delta'_w, \\ \psi(0) &= 0, & \left. \frac{\partial \psi(s)}{\partial s} \right|_{s=1} &= \frac{1}{2} \alpha' \delta'_v, \end{aligned} \quad (3.5)$$

where the free end conditions are originated in the semi-tangential torque [30] as discussed above. Using the complex function r , the boundary conditions above can be expressed as

$$r(0) = 0, \quad \left. \frac{\partial r(s)}{\partial s} \right|_{s=1} = \frac{1}{2}i\alpha' r_1, \quad (3.6)$$

where $r_1 = \delta'_v + i\delta'_w$.

In addition, we are able to specify a linear connection between an assumed displacement function $d(s)$ and $r(s)$ (see Fig. 3.2 b))

$$\frac{\partial d(s)}{\partial s} = r(s) \quad (3.7)$$

where $d(s) = v(s) + iw(s)$. It provides three additional conditions

$$d(0) = 0, \quad d(1) = d_1, \quad \left. \frac{\partial d(s)}{\partial s} \right|_{s=1} = r_1, \quad (3.8)$$

for the complex form Eq. (3.4) when it is transformed for $d(s)$.

3.2 Stability

The general solution of Eq. (3.4) is given by

$$r(s) = Ae^{\lambda_1 s} + Be^{\lambda_2 s} - \frac{\chi}{\gamma'} d_1, \quad \lambda_{1,2} = (\mu \pm \nu)i, \quad (3.9)$$

$$\mu = \alpha'/2, \quad \nu = \sqrt{\alpha'^2 + 4\gamma'}/2,$$

where $\lambda_{1,2}$ are purely imaginary eigenvalues. Applying Eq. (3.6), the unknown coefficients A, B are given by

$$A = \frac{\chi}{\gamma'} d_1 - \frac{\frac{1}{2}i\alpha' r_1 - \frac{\chi}{\gamma'} d_1 \lambda_1 e^{\lambda_1}}{\lambda_2 e^{\lambda_2} - \lambda_1 e^{\lambda_1}}, \quad B = \frac{\frac{1}{2}i\alpha' r_1 - \frac{\chi}{\gamma'} d_1 \lambda_1 e^{\lambda_1}}{\lambda_2 e^{\lambda_2} - \lambda_1 e^{\lambda_1}}. \quad (3.10)$$

In view of Eq. (3.7), the function $d(s)$ is then given by

$$d(s) = A \frac{e^{\lambda_1 s}}{\lambda_1} + B \frac{e^{\lambda_2 s}}{\lambda_2} - \frac{\chi}{\gamma'} d_1 s + C. \quad (3.11)$$

By means of Eq. (3.8), we could eliminate d_1 and r_1 , to find

$$\frac{\chi}{\gamma'} = \frac{\frac{e^{\lambda_2} (i\alpha' - 2\lambda_2) - e^{\lambda_1} (i\alpha' - 2\lambda_1)}{i\alpha' \left(\frac{1 - e^{\lambda_1}}{\lambda_1} + 1 \right) (e^{\lambda_1} - e^{\lambda_2})}}{1 + \frac{\lambda_2 (1 - e^{\lambda_1}) - \lambda_1 (1 - e^{\lambda_2})}{\lambda_1 \lambda_2 \left(\frac{1 - e^{\lambda_1}}{\lambda_1} + 1 \right) \left(\frac{e^{\lambda_1} - e^{\lambda_2}}{1 - e^{\lambda_1}} \right)} + \frac{\lambda_2^2 e^{\lambda_2} (1 - e^{\lambda_1} + \lambda_1) - \lambda_1^2 e^{\lambda_1} (1 - e^{\lambda_2} + \lambda_2)}{\frac{i\alpha' \lambda_1 \lambda_2}{2} \left(\frac{1 - e^{\lambda_1}}{\lambda_1} + 1 \right) (e^{\lambda_1} - e^{\lambda_2})}}. \quad (3.12)$$

In order to proceed, we note that the right hand side of Eq. (3.12) is in the form

$$\frac{\chi}{\gamma'} = \frac{P_r + iP_i}{Q_r + iQ_i} \quad (3.13)$$

where P_r, P_i and Q_r, Q_i are real quantities. Now the left hand side of Eq. (3.12) is real. So the right hand side of Eq. (3.13) must also be real and so its imaginary part has to vanish. Hence

$$P_i Q_r - P_r Q_i = 0. \quad (3.14)$$

But then the real part of the right hand side of Eq. (3.13) can be simplified so that we find

$$\frac{\chi}{\gamma'} = \frac{P_r}{Q_r}. \quad (3.15)$$

So using Eq. (3.15), Eq. (3.12) simplifies greatly to become

$$\chi = -\frac{\gamma'^2 \nu \cos \nu}{\alpha' \nu \sin \mu + \gamma' \nu \cos \nu - (2\nu^2 - \gamma') \sin \nu}. \quad (3.16)$$

3.3 Results

Eq. (3.16) is the main result of this problem. It denotes the relationship between rotation, compression and torsion and generates stability boundaries for the system. When α' tends to zero, we have $\mu = 0$, $\nu = \sqrt{\gamma'}$ and so we obtain Wang's result [29], that is, the case of a two-dimensional problem investigating a compressed, rotating beam in the absence of torsion

$$\chi = -\frac{\gamma' \sqrt{\gamma'} \cos \sqrt{\gamma'}}{\sqrt{\gamma'} \cos \sqrt{\gamma'} - \sin \sqrt{\gamma'}} \quad (3.17)$$

shown in Fig. 3.3 a). The stability boundaries are slightly curved. Boundary 1 is asymptotic to the line $\chi = -\gamma'$ and boundaries 2, 3 are asymptotic to the

values of $\gamma'_2 = 20.191$ and $\gamma'_3 = 59.679$, that are obtained from Eq. (3.17), when χ tends to infinity, that is

$$\sqrt{\gamma'} \cos \sqrt{\gamma'} = \sin \sqrt{\gamma'}.$$

When γ' tends to zero ($\alpha' \neq 0$), that is, the relative importance of gravity is negligible, we have that $\mu = \nu = \alpha'/2$ and hence from Eq. (3.16) by using L'Hospital's rule

$$\chi = \frac{\alpha'^3}{2(1 + \mu^2) \tan \mu - \alpha'}, \quad (3.18)$$

the stability boundaries can be seen in Fig. 3.3 b). Boundary 1 tends to the line $\chi = 3$ and boundaries are asymptotic to the values of $\alpha'_2 = 6.811$ and $\alpha'_3 = 12.868$, obtained from Eq. (3.18), when χ tends to infinity, that is

$$2(1 + \mu^2) \tan \mu = \alpha'.$$

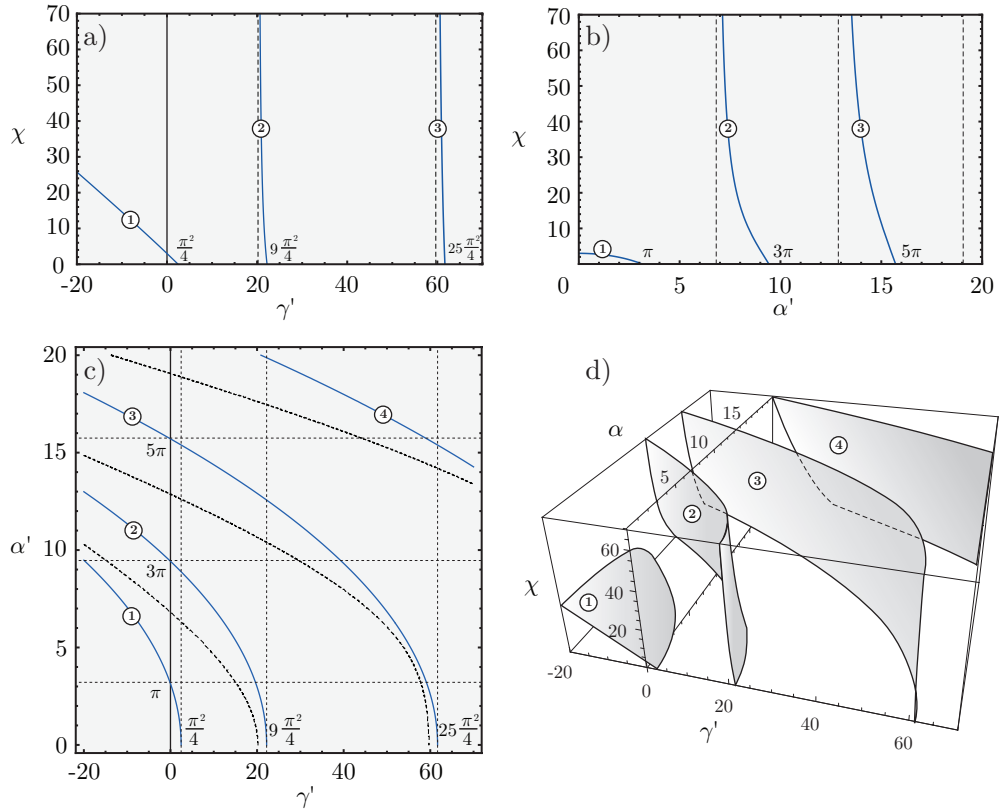


Figure 3.3: a) Stability boundaries in $(\chi - \gamma')$ plane. b) Stability boundaries in $(\chi - \alpha')$ plane. (c) Stability boundaries in $(\alpha' - \gamma')$ plane. d) 3D stability boundaries.

When χ might be neglected, the stability boundaries can be seen in Fig. 3.3 c). They are parabolic. The roots along the γ' axis are the well-known, normalized Euler buckling modes $(2n + 1)^2\pi^2/4$ where $n = 0, 1, \dots$, and along the α' axis are the normalized critical loads in terms of semi-tangential torque $(2n + 1)\pi$ where $n = 0, 1, \dots$.

The stability boundaries of the system, corresponding to Eq. (3.16) are depicted by Fig. 3.3 d). The curvature of the stability boundaries is continuously increasing as the parameter α' grows. They are asymptotic to the dashed lines. Looking again at Fig. 3.3 a), surface 1 crosses the χ axis at $\chi = 3$ (see Fig. 3.4). The system is absolutely stable as long as the solution does not reach the surface 1. Between surface 1 and 2 instability of the first mode might occur depending on whether the beam stands upward or downward. To the right of surface 2, 3 and 4 the instabilities of the second, third and fourth modes may occur. The validity of the stable and unstable modes are affected by torsion because it bends the stability boundaries as we can see in Fig. 3.3 c).

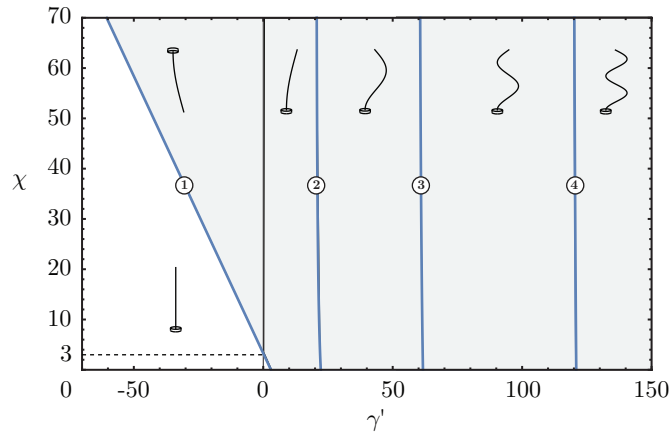


Figure 3.4: Explanation of stable and unstable modes.

Chapter 4

Laboratory tests

In order to identify precisely the effect of the longitudinal displacement ξ of a cantilever beam (see Sec. 1.4) on the natural frequency of the bending vibration, an experimental set-up was built (see Fig. 4.1). In case of three different beam lengths, the natural frequencies were measured while the beam was in the vertical position under either compression or tension (depending on whether it stood upward or downward).

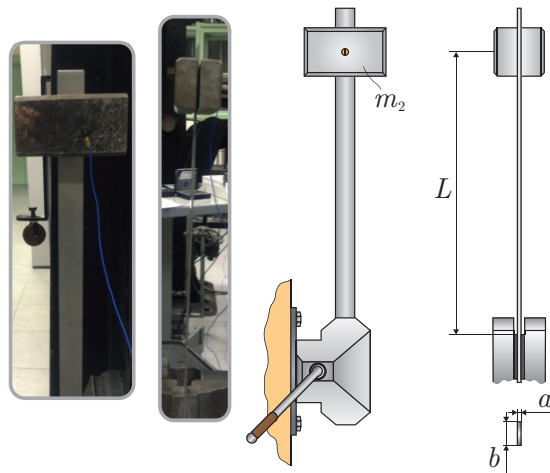


Figure 4.1: The experimental equipment that consists of a rectangular cross rod with length L and a heavy block with mass $m_2 = 0.978$ kg.

The horizontal position defined the neutral case, that is, the beam is not affected by the heavy block. The results of the experiment are summarised in Table 4.1. The average 15% difference of the frequencies depending on the longitudinal load type compared to the neutral case gives the motivation to investigate the problem deeply because there exist some industrial projects

where simple closed form expressions are needed for the calculation of the natural frequency of a cantilever beam with a heavy mass attached to its end, which takes into account whether the beam is vertical or horizontal [7].

Table 4.1: Measured natural frequencies. Three cases of load type are given.

Beam Length (m)	Compression (Hz)	Neutral (Hz)	Tension (Hz)
0.30	2.513	2.720	2.910
0.40	1.525	1.750	1.950
0.50	0.975	1.231	1.460

4.1 Bifurcation diagram

In Chap. 2, the models use a beam with absolutely straight axis meaning that the applied loads act exactly at the centre of gravity of the cross section. However, this theory cannot be realised experimentally in the reality because the point of the application of these loads has a certain eccentricity that influences the equivalent stiffness of the system.

Accordingly, we need to investigate the behaviour of an equivalent, one degree of freedom, nonlinear system to provide further explanation for the small discrepancies between the measurements and analytical results. The nonlinear model consists of a pinned-free rod and a torsional spring at the pinned end depicted in Fig. 4.2 b). Since the model is assumed to be equivalent, it is needed to fit the appropriate parameters θ_O and s_t to the measured system (see Fig. 4.1).

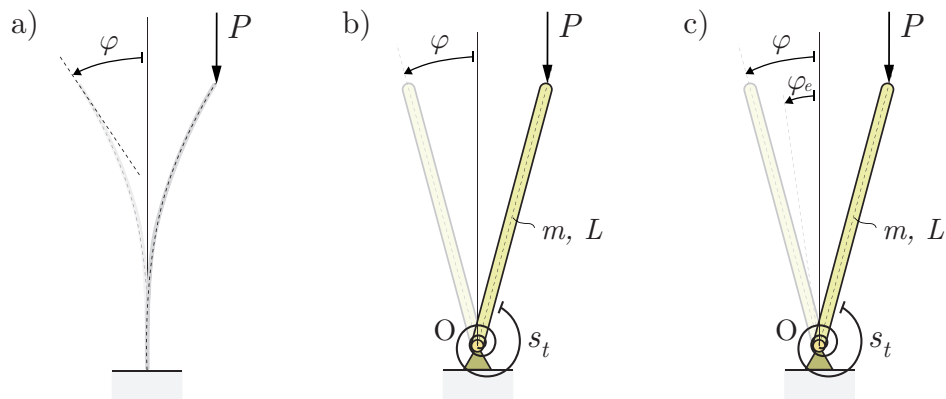


Figure 4.2: a) Compressed rod. b) Equivalent, nonlinear dynamical model of a compressed rod. c) Nonlinear dynamical model with angular error φ_e .

The torque balance of the nonlinear system assumes the form

$$-\theta_0 \ddot{\varphi}(t) = s_t \varphi(t) - PL \sin \varphi(t). \quad (4.1)$$

By linearising Eq. (4.1), we obtain

$$\theta_0 \ddot{\varphi}(t) + (s_t - PL)\varphi(t) = 0, \quad (4.2)$$

where the natural angular frequency of the system is

$$\omega_n = \sqrt{\frac{s_t - PL}{\theta_0}}. \quad (4.3)$$

It can be seen that when $s_t < PL$, the system becomes unstable as depicted in Fig. 4.3.

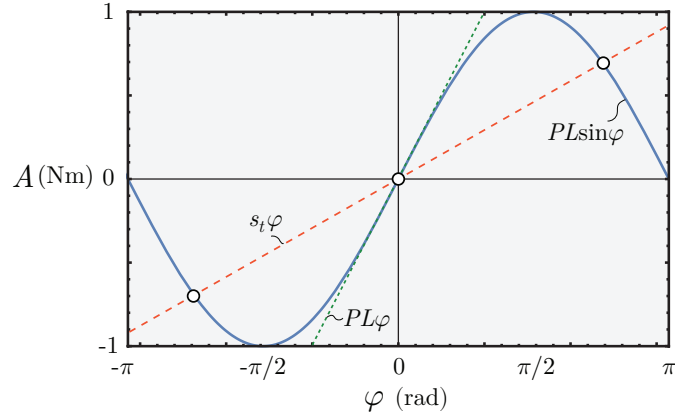


Figure 4.3: Linearising the equation of motion and investigating the possible roots.

If we investigate the stability boundary of the system that is given by

$$PL \sin \varphi = s_t \varphi \quad (4.4)$$

and the trigonometric function is substituted by its power series with respect to the angular rotation φ , then we obtain

$$PL \left(\varphi - \frac{1}{6} \varphi^3 \right) = s_t \varphi. \quad (4.5)$$

The simplification of Eq. (4.5) gives

$$\varphi^3 + \frac{6}{PL} (s_t - PL) \varphi = 0, \quad (4.6)$$

where the value of φ can be determined

$$\varphi_1 = 0, \quad \varphi_{2,3} = \pm \sqrt{\frac{6}{PL}(PL - s_t)}. \quad (4.7)$$

The bifurcation diagram of the system can be seen in Fig. 4.4.

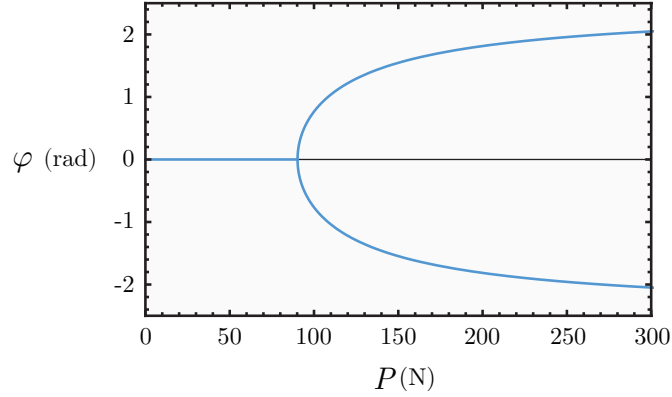


Figure 4.4: Bifurcation diagram ($s_t = 27.070$ Nm/rad, $\theta_O = 0.097$ kgm², $L = 0.30$ m).

During the measurements, probably we cannot assure that the axis of the rod is perfectly straight, thus we assume that the system has a certain angular error ($\varphi_e \neq 0$), which modifies the condition of stability (see also in Fig. 4.2 c)). In case of angular error, the equation of motion of the nonlinear system is given by

$$\ddot{\varphi}(t) + \frac{s_t}{\theta_O}(\varphi(t) - \varphi_e) - \frac{PL}{\theta_O} \sin \varphi(t) = 0, \quad (4.8)$$

After substituting the trigonometric function by its power series, we can examine the new condition of equilibria

$$PL \left(\varphi - \frac{1}{6}\varphi^3 \right) = s_t(\varphi - \varphi_e), \quad (4.9)$$

from which we obtain a cubic expression

$$\varphi^3 + \frac{6(s_t - PL)}{PL}\varphi - \frac{6s_t}{PL}\varphi_e = 0. \quad (4.10)$$

By using Cardano's theory, we can determine the roots of Eq. (4.10):

$$\varphi_1(P) = \frac{2\Upsilon\psi + \left(3\Upsilon^3 s_t \varphi_e + \sqrt{\Upsilon^3 (9\Upsilon s_t^2 \varphi_e^2 - 8\psi^3)} \right)^{2/3}}{\Upsilon (3\Upsilon^2 s_t \varphi_e + \sqrt{\Upsilon^3 (9\Upsilon s_t^2 \varphi_e^2 - 8\psi^3)})^{1/3}} \quad (4.11)$$

and

$$\varphi_{2,3}(P) = \frac{(1 \pm \sqrt{3}i) \left(\frac{1}{2\Upsilon} \left(3\Upsilon^3 s_t \varphi_e + \sqrt{\Upsilon^3 (9\Upsilon s_t^2 \varphi_e^2 - 8\psi^3)} \right)^{2/3} - \psi \right)}{(3\Upsilon^2 s_t \varphi_e + \sqrt{\Upsilon^3 (9\Upsilon s_t^2 \varphi_e^2 - 8\psi^3)})^{1/3}}, \quad (4.12)$$

where $\Upsilon = PL$ and $\psi = PL - s_t$. Based on the expressions of Eqs. (4.11) and (4.12) where P is also emphasized, the bifurcation diagram can be seen Fig. 4.5 in terms of the angular error φ_e .

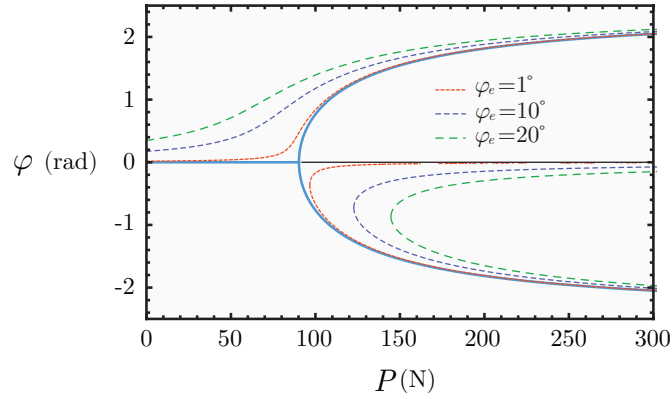


Figure 4.5: Bifurcation diagram in terms of angular error ($s_t = 27.070$ Nm/rad, $\theta_O = 0.097$ kgm², $L = 0.30$ m).

To investigate the variation of the natural angular frequencies of the system, we need to transform the equation of motion of the system to the form of small perturbation. The small disturbance can be defined as

$$\varphi(t) = \varphi_1(P) + x(t). \quad (4.13)$$

Substituting this into Eq. (4.8), after the linearisation, we obtain

$$\ddot{x}(t) + \frac{s_t + PL \left(\frac{1}{2}\varphi_1(P) - 1 \right)}{\theta_O} x(t) + s_t(\varphi_1(P) - \varphi_e) \quad (4.14)$$

$$- \frac{PL}{\theta_O} \left(\varphi_1(P) + \frac{1}{6}\varphi_1^3(P) \right) = 0.$$

In the linearised equation, $x(t) = 0$ is the trivial solution, which corresponds to the asymmetric $\varphi_1(P)$ equilibrium position. If we consider the exact value

of $\varphi_1(P)$, then Eq. (4.14) can be transformed to the form of $\ddot{x}(t) + \omega_n^2 x(t) = 0$. The natural angular frequency ω_n of the system can be seen in Fig. 4.6.

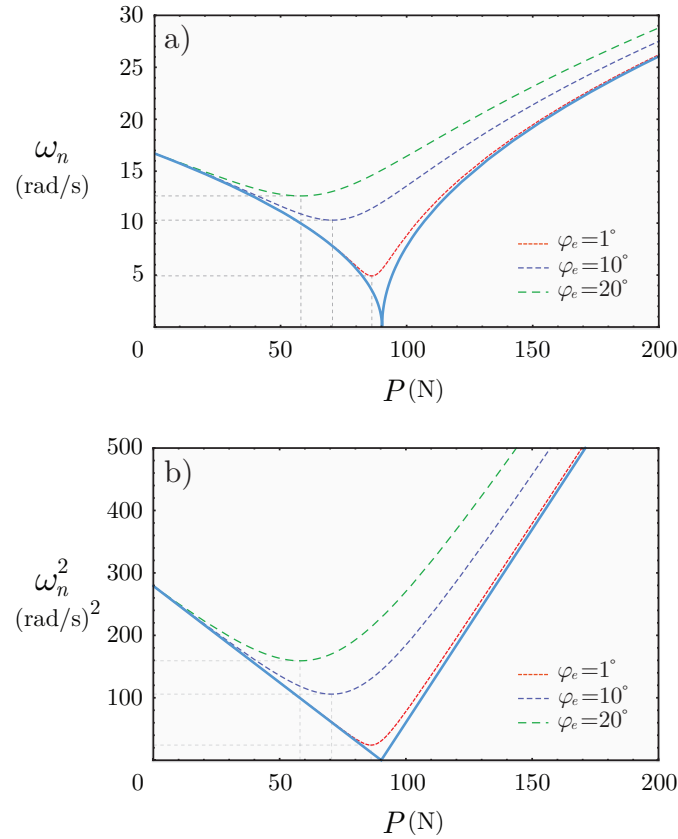


Figure 4.6: a) Natural angular frequency with angular error b) Natural angular frequency squared with angle error ($s_t = 27.070$ Nm/rad, $\theta_O = 0.097$ kgm², $L = 0.30$ m).

As we know, the relationship between compression and the square of the natural angular frequency is linear, which statement is also shown by in Fig. 4.6 b). If we consider the case of $\varphi_e = 20^\circ$, we can see that this error is the largest. Still, since the compressive force is only cca. 10 N (see Fig. 4.1), it means only 0.55% discrepancy in the frequency. The biggest discrepancies can be found at the minimum point of the curves at around 50-100 N compared to the case with no angular error.

In reality, buckling occurs as the function of the angular error as it is described by the problem. Basically, we do not experience a sudden collapse at the critical value of the load, rather a slight, climbing deflection that

appears already before reaching the critical value.

Table 4.2: Characteristic points of the functions of Fig. 4.6 a) .

Angular error (°)	Minimum of the function	
	ω_n (rad/s)	P (N)
1	4.923	86.198
10	10.288	70.591
20	12.619	58.064

Table 4.3: Characteristic points of the functions of Fig. 4.6 b) .

Angular error (°)	Minimum of the function	
	ω_n (rad/s)	P (N)
1	24.238	86.198
10	105.845	70.591
20	159.249	58.064

4.2 Experimental results

To provide analytical results, let us use Eq. (2.25). While Eq. (2.25) provides only results concerning compression, the end mass is able to behave as tension where the natural frequencies are also easily calculated. If the acceleration of gravity assumed to be zero then we obtain the neutral case where the experimental equipment is held horizontally. The results of the compressed, tensed and neutral beam are summarized in Table 4.5 by different beam lengths.

First of all, we can realise that the natural frequencies are lower in compression compared to the neutral case because it decreases the stiffness of the cantilever beam. On the other hand tension increases the stiffness that causes higher natural frequencies. The natural frequencies also depend on the length of the beam.

The error columns of Table 4.5 mean the difference between the analytical and measured results (see Table 4.1). It can be seen that the largest relative error is not greater than 4 %. These minor discrepancies might be caused by the asymmetric disposition of the experimental equipment depending on the length of the beam, too [7].

If we take a look at the results of the nonlinear model, then it can be seen that the relative error is zero when the angle error is zero. This is because the mechanical parameters of the model was fitted to the natural frequencies of the measured system. If we increase the angle error, we experience only minor discrepancies compared to the case devoid of error.

Note that in case of the nonlinear system, the torsional spring stiffness s_t and the mass moment of inertia θ_O are fitted to the measured system ($s_t = 3IE/L$ and θ_O is also fitted by means of Eq. (4.3)). The effect of the fitted parameters is manifested in the shifted critical load of the system.

Table 4.4: Experimental data for Fig. 4.1.

Notation	Designation	Value	Unit
ρ	Density of beam	7900	kg/m ³
E	Young's modulus of beam	200	GPa
a	Thickness of cross section	0.0020	m
b	Width of cross section	0.0203	m
L	Length of beam	0.30; 0.40; 0.50	m
m_2	Mass of end body	0.978	kg
m_0	Mass of beam	0.096; 0.128; 0.160	kg
θ_C	Moment of inertia of end body	0.00028	kgm ²
–	Size of end body (one block)	0.0187×0.0792×0.0427	m×m×m

Table 4.5: Analytical results for the first natural frequency of the system. The error columns mean the difference from the measured results that can be seen in Table 4.1.

Beam Length (m)	Compression		Neutral		Tension	
	Results (Hz)	Error (%)	Results (Hz)	Error (%)	Results (Hz)	Error (%)
0.30	2.563	1.99	2.749	1.07	2.923	0.45
0.40	1.559	2.23	1.782	1.83	1.978	1.44
0.50	1.008	3.27	1.271	3.25	1.486	1.78

Table 4.6: Analytical results of the nonlinear system depending on the rate of the angular error. The error columns mean the difference from the measured results that can be seen in Table 4.1.

Beam Length (m)	0.3			0.4			0.5		
Angular error (°)	0	10	20	0	10	20	0	10	20
Natural frequency (Hz)	2.513	2.516	2.527	1.525	1.529	1.545	0.975	0.982	1.005
Error (%)	0	0.12	0.56	0	0.26	1.31	0	0.72	3.08

Summary

The objective of the thesis was to determine the mechanical behaviour of a cantilever beam subjected to combined loads such as compression, tension and torsion. The motivation was the precise calculation of natural frequencies in case of long boring bars. First of all, it was needed to propose the way how to investigate the problem in the presence of the applied loads. Two different cases were separated, the equilibrium approach and the kinetic approach. The equilibrium approach assumes that the observation is needed to be done by means of a nontrivial equilibrium configuration in the vicinity of the trivial equilibrium. In contrast, the kinetic approach is to figure out whether the small perturbation of the equilibrium configuration results in motion or not. Since the approaches provided different solutions in case of axial torsion, we had to introduce a new type of torsion called semi-tangential torsion [30]. It meant the appropriate way to maintain the stability issues by means of the equilibrium approach, thus the deformation functions using this were subjected to further investigation.

In course of the task, three dynamical models had been analysed in detail including compression, tension and torsion. The purpose was to specify the natural frequencies of the systems by using the theory of lateral stiffness variation. One of the models brings up a classical topic of beam theory, which assumes that the displacement ξ in the beam direction might be neglected because that is a second order function $\xi = \kappa\eta^2$ of the lateral displacement η . In terms of vibration theory, the longitudinal lifting of the end point of the beam causes a variation in the potential function of the system that has an influence on the natural frequencies. The investigated formula is given by its power series

$$\kappa L = \frac{3}{5} + \frac{1}{175} \left(\frac{L^2 P}{IE} \right) + \frac{1}{2625} \left(\frac{L^2 P}{IE} \right)^2 + \dots,$$

that makes up connection between the longitudinal and lateral displacements of the end of the beam in case of compressive force P .

The question was whether the modification of the potential energy corresponds to the stiffness variation of the system under the combined loads

above. By means of Betti's Theorem, it can be proved that the work of external loads using the longitudinal displacement equals to the strain energy function of the system considered only by bending.

Since our investigation is connected to the vibration of boring tools, we also had to take into account a rotating system. The tool is modelled by a rotating cantilever beam that is subject to compression and torsion, manifested by semi-tangential torque. The three dimensional model is based on the linear Euler-Bernoulli beam theory. Finally, we obtained a dimensionless relationship between the relative importance of rotation, compression, and torsion that reveals the stability boundaries of the system.

To validate our results related to the potential energy variation of the beam, an experimental equipment was designed and constructed. As we could see, the analytical results correspond to the measurement results where the slight errors might be explained by the asymmetric disposition of the device that was investigated by a one degree of freedom nonlinear model. Graff [13] has also examined the dynamics of beams and elaborated on the flexural waves in thin rods under different types of loads. He dealt with the effects of prestress in case of a pin-ended column investigating continuum beam without end mass. The development of his models might provide another way to understand our results.

In conclusion, the importance of our potential energy variation theory is manifested by the natural frequency calculations of the blades of wind turbines and long boring tools [16, 17, 19, 10, 11] where large longitudinal forces might appear. There are many related theoretical, numerical results and topics in the literature: Bayly *et al.* [2] investigated the low frequency vibration in drilling to find agreement with drilling tests in the presence of large longitudinal cutting forces. Roukema, Altintas [23] and Heisig, Neubert [15] also considered lateral vibration of drilling tools. Park *et al.* [22] examined the linear vibration of blades of a wind-turbine to see how to avoid structural resonance due to significant axial forces caused by rotation.

Keywords: torsion, compression, potential energy, stability

Összefoglalás

A dolgozat célkitűzése annak a megállapítása volt, hogy egy befogott tartó hogyan viselkedik összetett terhelés hatására. A vizsgálatokat hosszú fúrórúdak sajátfrekvenciáinak pontos meghatározása motiválta. A vizsgálat nyomó, húzó és csavaró terhelésekre terjedt ki. A feladat első lépésében a rendszer stabilitásának vizsgálatával foglalkoztam, melyre az irodalom két különböző vizsgálati módszert emel ki: az egyensúlyi, illetve a dinamikai megközelítést [30]. Az egyensúlyi megközelítés azt feltételezi, hogy a rendszer vizsgálatát egy, a triviális egyensúlyi helyzetének környezetében megjelenő nem triviális egyensúlyi helyzet alapján végezzük. Ezzel szemben a dinamikai megközelítés kis perturbációs módszert használ annak érdekében, hogy kiderítse, hogy az egyensúlyban lévő rendszer ezen kis perturbáció hatására hogyan viselkedik. Mivel a két stabilitási elmélet különböző megoldást szolgáltat egy tisztán, axiálisan csavart befogott rúd esetében, így a csavarás rúdra való átadásának vizsgálatára volt szükség. A dolgozat az irodalomban fellelhető szemintangenciális nyomatókkal foglalkozott [30] az egyensúlyi módszer alapján.

A feladat során három mechanikai modell részletes vizsgálatával foglalkoztam, ahol megkülönböztetünk nyomó, húzó, csavaró és ezek kombinációból adódó terheléseket. A cél annak a meghatározása volt, hogy ezen terhelések hatására hogyan változik a rendszer sajátfrekvenciája. A vizsgálat itt ugyancsak két részre bontható. Főként a rendszer merevségváltozásával foglalkoztam, de megjelent egy, a rendszer helyzeti energiájának változásával foglalkozó elmélet is. Ez az elmélet azt feltételezi, hogy egy függőleges helyzetben álló rúd tengelyére merőleges irányú erő hatására nem csupán erőirányú, hanem rúdirányú elmozdulás is bekövetkezik. A rúdirányú ξ elmozdulás és az erőirányú η elmozdulás kapcsolata másodrendű $\xi = \kappa\eta^2$. Rezgéstani értelemben a rúd végének függőleges irányú elmozdulása megváltoztatja a rendszer potenciális energiáját és így befolyásolja annak sajátfrekvenciáját. Itt κ meghatározása volt a cél laterális és nyomó terhelés hatása alatt. A vizsgált formula a következő dimenziótlanított MacLaurin-sor formájában

adható meg

$$\kappa L = \frac{3}{5} + \frac{1}{175} \left(\frac{L^2 P}{IE} \right) + \frac{1}{2625} \left(\frac{L^2 P}{IE} \right)^2 + \dots,$$

ahol P a nyomóerőt jelenti. Felmerült a kérdés, hogy a potenciális energia megváltozása, illetve a rendszer merevségének adott terhelés hatására történő megváltozása milyen kapcsolatban vannak egymással. A Betti-tétel segítségével bebizonyítottam, hogy a külső erők munkája és a rendszer alakváltozási energiája megegyezik.

Mivel mechanikai modelljeink arra hivatottak, hogy egy fűrőszerszámot modellezzenek, így figyelmet kellett fordítani a rendszer forgására is. A szer-szám ekkor egy, az Euler-Bernoulli rúdelméleten alapuló, forgó befogott tartóként volt modellezve, melyre nyomó és csavaró terhelések hatnak. A rendszer vizsgálata egy dimenziómentes stabilitási térképhez vezetett, mely kapcsolatot teremt a nyomás, a csavarás és a szögsebesség között.

Annak érdekében, hogy validálni tudjam a rendszer potenciális energiájának megváltozásához köthető eredményeinket, egy korábban készített kísérleti eszköz sajátfrekvenciáit mértem [7]. Az analitikus eredmények jó közelítéssel megfeleltek a mért eredményinknek. A tapasztalt kis mértékű eltérések magyarázataként egy egy szabadsági fokú nemlineáris rendszer vizsgálatával is foglalkoztam, mivel felvetődött, hogy a kísérleti eszköz aszimmetrikus helyzete (kezdeti szöghibája) befolyásolhatja a rendszer sajátfrekvenciáit. Az irodalomban is fellelhetőek ezzel kapcsolatos kutatások. Graff [13] ugyancsak rudak dinamikai viselkedésével foglalkozott és vizsgálta, hogy a hajlító hullámok hogyan terjednek vékony, különbözően terhelt rudakban.

Összegzésként elmondható, hogy a dolgozatban taglalt téma szoros kapcsolatban áll turbinalapátok és hosszú fűrőszerszámok sajátfrekvenciáinak meghatározásával [16, 17, 19, 10, 11]. Számos kapcsolódó elméleti és numerikus eredmény is fellelhető az irodalomban, mint például Bayly [2], aki a fűrész alacsony frekvenciás rezgését vizsgálta mind elméleti, mind pedig gyakorlati vonatkozásban. Roukema, Altintas [23] Heisig és Neubert [15] ugyancsak laterális rezgéseket vizsgáltak fűrőrudak tekintetében. Park [22] és mások pedig turbinalapátok lineáris rezgéseivel foglalkozott annak érdekében, hogy megoldást találjon a rezonancia elkerülésére.

Bibliography

- [1] Adamowitz, M.; Stegun, I. A. Handbook of Mathematical Functions with Formulas, Graphs and Mathematical Tables (1972). pp. 11.
- [2] Bayly, P., Lamar, M., and Calvert, S., Low frequency regenerative vibration and the formation of lobed holes in drilling. *Journal of Manufacturing Science and Engineering*, 124(2), April, (2002) pp. 275–285.
- [3] Bazǎnt, Zdeněk; Cedolin, Luigi. Stability of Structures. *World Scientific Publishing Co. Pte. Ltd.* (2010).
- [4] Beck, M. Knickung gerader Stabe durch Druck und konservative Torsion. *Springer.* (1955).
- [5] Beléndez, T.; Neipp, C.; Beléndez, A. Large and small deflections of a cantilever beam. *European Journal of Physics*. Vol. 23, No. 3 (May 2002). pp. 371-379.
- [6] Beri, B., Stepan, G., Hogan, S.J., Effect of potential energy variation on the natural frequency of an Euler-Bernoulli cantilever beam under lateral force and compression. *Journal of Applied Mechanics*, 84(5), May, (2017), no. 051002 pp. 1-8.
- [7] Beri, B. Gravitációs erőtér hatásának elemzése rudak hajlítólengéseire (2014).
- [8] Borboni, A.; De Santis, D. Large deflection of a non-linear, elastic, asymmetric Ludwick cantilever beam subjected to horizontal force, vertical force and bending torque at the free end. *Meccanica*. Vol. 49, No. 6 (June 2014). pp. 1327-1336.
- [9] Cooke, JR.; Rand, RH. Vibratory Fruit Harvesting: A Linear Theory of Fruit-stem Dynamics. *Journal of Agricultural Engineering Research*. Vol. 14, No. 3 (1969). pp. 195-209.

-
- [10] Ema, S., and Marui, E., Suppression of chatter vibration of boring tools using impact dampers. *International Journal of Machine Tools and Manufacture*, 40(8), June, (2000) pp. 1141–1156.
- [11] Ema, S., and Marui, E., Theoretical analysis on chatter vibration in drilling and its suppression. *Journal of Materials Processing Technology*, 138(1-3), July, (2003) pp. 572–578.
- [12] González, C.; LLorca, J. Stiffness of a curved beam subjected to axial load and large displacements. *International Journal of Solids and Structures*. Vol. 42, No. 5-6 (March 2005). pp. 1537-1545.
- [13] Graff, K. Wave motion in Elastic Solids. *Dover Publication Inc., New York*. (1975).
- [14] Greenhill, A. G. On the Strength of Shafting When Exposed Both to Torsion and to End Thrust . Vol. 34, No. 1 *Proceedings of the Institution of Mechanical Engineers*. (April 1883). pp. 182-225.
- [15] Heisig, G., and Neubert, M., Lateral drillstring vibrations in extended-reach wells. *Society of Petroleum Engineers*, February, (2000).
- [16] Jureczko, M., Pawlak, M., and Mezyk, A., Optimisation of wind turbine blades. *Journal of Materials Processing Technology*, 167(2-3), August, (2005) pp. 463– 471.
- [17] Kong, C., Bang, J., and Sugiyama, Y., Structural investigation of composite wind turbine blade considering various load cases and fatigue life. *Energy*, 30(11- 12), August, (2005) pp. 2101–2114.
- [18] Lee, K. Large deflections of cantilever beams of non-linear elastic material under a combined loading. *International Journal of Non-Linear Mechanics*. Vol. 37, No. 3 (April 2002). pp. 439-443.
- [19] Lee, D., Hwang, H., and Kim, J., Design and manufacture of a carbon fiber epoxy rotating boring bar. *Composite Structures*, 60(1), April, (2003) pp. 115–124.
- [20] Ludvig, Gy. Gépek dinamikája *Műszaki Könyvkiadó*. (1973).
- [21] Muttnyánszky, Á. Szilárdságtan. *Műszaki Könyvkiadó*. (1981).
- [22] Park, J., Park, H., Jeong, S., Lee, S., Shin, Y., and Park, J., Linear vibration analysis of rotating wind turbine blade. *Current Applied Physics*, 10(9), March, (2010) pp. S332–S334.

- [23] Roukema, J., and Altintas, Y., Generalized modeling of drilling vibrations. part ii: Chatter stability in frequency domain. *International Journal of Machine Tools and Manufacture*, 47(9), July, (2007) pp. 1474–1485.
- [24] Serope, K.; Schmid, S. Manufacturing, Engineering and Technology. *Prentice Hall*. (August 2005) pp. 22–36, 951–988.
- [25] Solano-Carrillo, E. Semi-exact solutions for large deflections of cantilever beams of non-linear elastic behaviour. *International Journal of Non-Linear Mechanics*. Vol. 42, No. 2 (March 2009). pp. 253-256.
- [26] Stepan, G.; Csernák G. A műszaki rezgésstan alapjai (2012).
- [27] Timoshenko, S. P.; Gere, J. M. Theory of Elastic Stability. *McGraw-Hill International Book Company*. (1963).
- [28] Troesch, A. Stabilitatprobleme bei tordierten Staben und Wellen. Vol. 20 *Ing. Arch.*. (March 1952). pp. 258.
- [29] Wang, C. Y. Stability of a light rotating column with an end mass . Vol. 43, No. 1 *Acta Mechanica*. (March 1982). pp. 137-139.
- [30] Ziegler, H. Principles of Structural Stability. *Blaisdell Pub. Co.*. (1968).
- [31] https://en.wikipedia.org/wiki/Machining_vibrations